Master's Thesis

Development of Graphene-Paper-Based Thermal Interface Materials

Daechan Jeon

Department of Mechanical Engineering

Graduate School of UNIST

2019

Development of Graphene-Paper-Based Thermal Interface Materials

Daechan Jeon

Department of Mechanical Engineering

Graduate School of UNIST

Development of Graphene-Paper-Based Thermal Interface Materials

A thesis/dissertation
submitted to the Graduate School of UNIST
in partial fulfillment of the
requirements for the degree of
Master of Science

Daechan Jeon

12. 21. 2018 Month/Day/Year of submission

Approved by

Advisor
Jaeseon Lee

Development of Graphene-Paper-Based Thermal Interface Materials

Daechan Jeon

This certifies that the thesis/dissertation of Daechan Jeon is approved.

12. 21. 2018 Month/Day/Year of submission

signature

Advisor: Jaeseon Lee

signature

Jaehwa Lee: Thesis Committee Member #1

signature

Jooha Kim: Thesis Committee Member #2

signature

typed name: Thesis Committee Member #3

signature

typed name: Thesis Committee Member #4;
three signatures total in case of masters

Abstract

Thin and lightweight heat spreader has gained a significant attention in semiconductor industry due to the miniaturization of electronic devices and the resulting high-density heat generation. In addition, the thermal interface materials (TIMs, hereafter) is also regarded as an essential component in the thermal management for reducing the thermal contact resistance. In regard to the TIM, the flexibility, versatility, as well as thermal performance are considered as important properties. In this study, a graphene paper based, thin and flexible TIM has been successfully fabricated by incorporating commercially-available papers with water-dispersible graphene paste (WDG). Various types of commercially-available papers: a Munken; a Matt; a Bulgyeong; a Daerye; a Merit; an Aqua satin; a Wool paper; and a New craft board which have the different characteristics are used to fabricate the graphene paper TIM via a simple and cost-effective ink coating process: dip coating; bar coating; and slot die coating. The cellulose with high mechanical strength forms interconnected networks with the graphene which can significantly improve the thermal and mechanical properties. Also, poly (vinyl butyral-co-vinyl alcohol-co-vinyl acetate) (P(VB-co-VA-co-VAc)) copolymer which is often used as an adhesive layer in the coating process is used for increasing the mechanical strength which is attributed to the strong hydrogen bonding interaction between the cellulose, copolymer, and graphene.

The in-plane and through-plane thermal conductivities of the graphene paper TIM are measured using a laser-flash-technique. The measured in-plane thermal conductivities are of the order of 5 W/m-K, which corresponds to 100 times increase of thermal conductivity compared to the pristine paper, whereas the through-plane thermal conductivities are of the order of 0.1 W/m-K. Especially, the graphene paper TIM with 25 wt% graphene shows an in-plane and through-plane thermal conductivity of 7.32 W/m-K and 0.14 W/m-K, respectively which are equal or even exceed those of conventional synthetic-plastics-based TIMs. These results suggest that the addition of graphene significantly enhance the in-plane thermal conductivity of papers, while the through-plane thermal conductivities are not significantly improved due to its two-dimensional crystal structure. In order to improve the through-plane thermal conductivity, a hybrid filler is used. The hybrid filler formulations resulted in a slight enhancement of the through-plane thermal conductivity by addition of microparticles fillers with spherical or elliptical configurations. The electrical and mechanical properties of the graphene paper TIM are also tested. The measured sheet resistance and tensile strength of graphene paper TIM are 508 ohm/sq and 33.86 MPa respectively, which are sufficient values for TIM. This work proposed a promising candidate for next-generation thermal interface materials with good thermal and mechanical properties.

Contents

List of Figures

List of Tables

Nomenclature

Symbol	***Description***	***Unit***
A	Area	[m^2]
C	Specific heat	[KJ/kg-K]
G	Graphene	[-]
I	Current	[A]
k	Thermal conductivity	[W/m-K]
L	Thickness of the sample	[m]
m	Mass	[kg]
P	Copolymer	[-]
p	Pressure	[kg/m-s^2]
Q	Input energy by laser pulse	[W]
R	Thermal resistance	[K/W]
S	Probe spacing	[m]
t	Time	[s]
T	Temperature	[K]
V	Voltage	[V]

Greek symbols

α	Thermal diffusivity	[mm^2/s]
ε	Porosity	[-]
ρ	Density	[kg/m^3]
ρ	Resistivity	[Ω-m]
V	Volume	[m^3]

Subscripts, Superscripts

C	Contact	[-]
max	Maximum	[-]
TIM	Thermal Interface Material	[-]
S	Sheet resistance	[-]
T	Total	[-]
t	Time	[-]
V	Void-space	[-]
’	Comparative sample	[-]

1. Introduction

Due to the development of industrial technology, there is a tendency that electronic devices are gradually reduced in weight, miniaturized, and integrated [1-3]. As a result, the size of the electronic components inevitably decreases. In this regard, the amounts of heat generation per unit area gradually increases [4]. It affects not only deteriorating the performance of the element but also causing malfunction of the element, deterioration of the substrate, shortening of the lifetime and cause problems such as lower reliability. Such trends are being gradually accelerated, increasing the demand for thermal management which improves the technology of electronic equipment and the need for technologies to effectively dissipate heat is gradually increased [33]. Recently, it is in various commercial electronic devices such as LED, touch panel, laptop, computer, high-performance CPU chipset, display, smartphone required appropriate thermal management system [5-7]. In these electronic devices, thin and lightweight heat spreader has gained a significant attention in semiconductor industry [32].

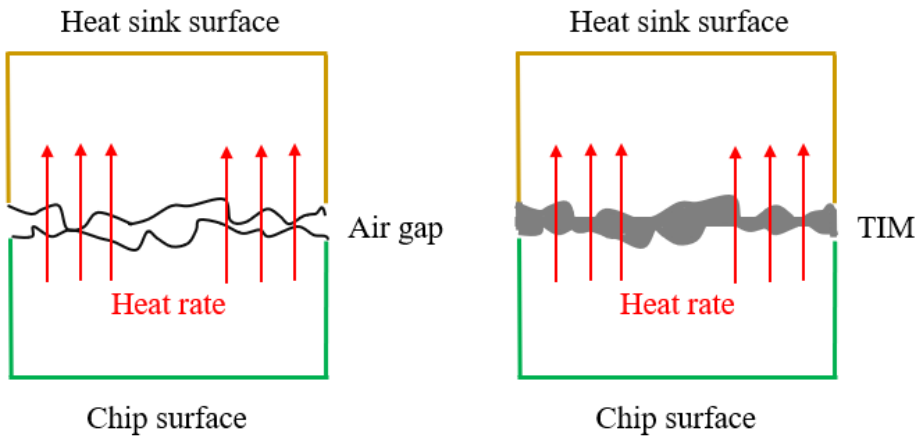

Figure 1.1. Illustration of the contact thermal resistance

In these thermal management systems, one of the major bottlenecks for the heat transfer path is the contact thermal resistance generated between the two mating rigid surfaces. The main factor in the thermal management application is to improve the heat transfer path for conduction in the interface between the materials which can be the serious bottlenecks for heat conduction which is important limited part important for improving the performance of electronic devices. When two solid surfaces are opposed to each other, each surface has an irregular pattern such as morphological surface roughness, waviness, and deviation. Therefore, it has a very limited small contact surface compared with the actual surfaces. In the meantime, it is separated into a void filled with air and the heat transfer to the interface

through the air with the thermal conductivity of air is about 0.02 W/m-K can be assumed almost ignored [8]. These voids interface with the thermal path and are indicated by the rapid temperature drop at the interface.

As a capable method for reducing these contact thermal resistances, i) Increasing contact pressure: this will even out peaks and valley and flatten distorted surfaces, and ii) Grinding or buffing surfaces: this will remove roughness factor between the surface and flatten grinding surface. However, there are also other disadvantages, i) Pressures which affect the surfaces will cause load constraint for electronic systems and ii) Manufacturing technologies for highly worked surfaces are not cost effective.

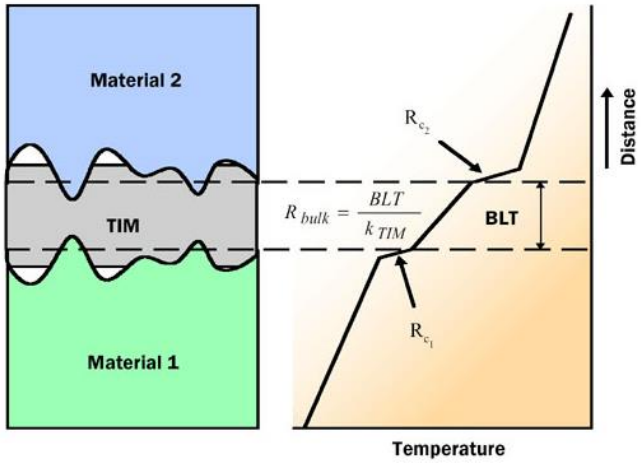

Figure 1.2. Configuration of the use for TIM

Therefore, the best way to reduce the contact thermal resistance in these cooling modules for electronic systems is to use the thermal interface materials (TIMs, hereafter) between the two mating rigid surfaces [9-11]. The TIMs describes any material which is inserted between the two mating rigid surfaces and parts for enhancement of the thermal application for that of two component parts. [27]. Thermal performance of TIMs is generally evaluated based on thermal interface resistance (R_{TIM}, hereafter). R_{TIM} is a measurement of how difficult it is for heat to be consumed at the between surfaces. R_{TIM} is the total thermal interface resistance which contact thermal resistance of the bottom surface (R_{C1}, hereafter) and contact thermal resistance in upper surface ($R_{C2,}$ hereafter) are contact thermal resistance in between the surfaces between the TIMs and the two mating rigid surfaces. The thermal conductivities of TIMs and bond line thickness (BLT, hereafter) means the thickness of an applied TIMs. Depending on the TIMs and the type of application, it can affect the overall performance [40]. Therefore, it is dependent on the identify what factors need to be optimized when choosing TIM or designing it is there [51].

R_C – Contact thermal resistance is generated between the substrate and the TIMs by the thermal contact. This contact resistance is limited to such a degree that TIMs well matches the substrate and fills the gap. This is influenced by compliance with TIMs and substrate adaption and depends greatly on the pressure applied to some TIMs.

BLT – The bond line thickness of TIMs is how the two faces are separated in which mean a measure of thick. Since TIMs typically have low thermal conductivity than any of the substrate, it is required to minimize BLT to reduce thermal resistance. In addition, when BLT is thin, the cost is generally cheap for a low amount of used material.

α – The thermal conductivities of the TIMs are the measure of how much heat is generated in the material itself. It is as the important element as high thermal conductivity as BLT.

Ideal TIM is composed of materials combining low BLT, high thermal conductivities, and the low thermal contact resistance [41-42]. On the other hands, when choosing or designing a TIMs separately from the thermal interface resistance, there are various parameters to consider such as electrical and mechanical properties. Whether the TIM is electrically insulated affects the problem of handling ability and stability of the TIM. In addition, in the case of mechanical properties, it is necessary to confirm whether it has sufficient mechanical properties to be used as a TIM due to adaptability problem, stability, reliability, and lifetime.

(a)

(b)

Figure 1.3. (a) Use of TIM in electronic components and (b) various types of commercially-available TIMs.

Currently, there are various kinds of TIMs as like commercially available thermal grease, elastomer pad, phase change materials (PCMs, hereafter), and adhesive. Thermal grease is a common use for the electronics systems. It is expected to have the very thin BLT and low thermal resistance in application. It has neither much mechanical strength nor does not need the external pressure for mechanical contact. Due to the unnecessary of curing properties, it is used only in which the material can consist, also in any application where the grease will allow viscosity to maintain for applicability for using the thermal grease. And, Thermal glue is expected to have the very thin BLT. However, thermal glue will additionally be required any contact pressure for the bonding after the curing process. Therefore, thermal glue allows thicker BLT than the thermal grease. Thermal gap filler might be represented, non-adhesive material such thermal glue, allows thicker BLT than the thermal grease still allowing the easy disassembly owing to the limited adhesiveness. As unlike to before TIM, the thermal

pad does not require for liquid and paste states, but for the form of solid. Most of silicone and silicone-like materials, it has the advantage of applied easily, and it can require thicker BLT but will also need higher mechanical force for contact pressure in heat sink which mating the heat source in order that the thermal pad conform to the between the mating two surfaces. Thermal adhesion is critically a thermal pad with adhesion properties for contact. Thermal tapes adhere to the surfaces, require no curing time and is easy for applying. PCMs, naturally adhesion materials for using as the replacement for the thermal greases or glue which have achievement of melting point – 50 to 60 degrees Celsius for changing to half liquid form and fill the gaps between the two mating rigid surfaces. In this way, various TIMs are widely used commercially and it is important to select and use an appropriate TIMs matching for each application.

Recently, various studies for the process of fabricating TIMs for the matrix and filler materials, characterization and development of fillers, and thermal characterization of TIMs are studying steadily. In this regard, the matrix for the various TIMs fabrication methods has been studied with cellulose as a base material [12-13]. Since most thermally conductive plastics such as polyamide, epoxy, and polypropylene used for TIMs is treated as a synthetic polymer based on petrochemical products. It ultimately occurs problem for economic and environmental aspects cause of the sustained concern. Therefore, the usability of environmental and renewable energy for producing the green plastic in excellent heat conduction ability increases its applicability. The most economical and promising temperament cellulose matrix is the common sufficient natural material of polymer matrix in the surroundings. Because cellulose has the excellent mechanical strength, transparency, and does not cause plastic deformation, cellulose based materials have various applicable uses for fields such as conductor, supercapacitors, biomaterials, and aerospace. Unlike ordinary plastics, cellulose-based plastic (CBP, hereafter) also has physical properties such with the excellent thermal stability, biodegradability, high tensile strength and possibility of regeneration [14]. These properties have excellent advantages for using TIMs matrix.

In addition, there are many studies for fabricating TIMs using graphene filler among various substances such as metal, ceramics, and carbon allotropes used as TIMs filler materials based on the cellulose [15-16]. Graphene is a crystal structure of monolayer of sp^2 bonded carbon atoms connected in a hexagon and has offered considerable interests in the efficient thermal management application for the TIM materials due to the extremely highly thermal properteis. Recently, graphene-based materials were studies about transparent, also flexible electrodes for lithium-ion batteries, supercapacitors, polymer composites, ultra-thin films, electronic circuits, displays, and solar cells. In addition, it is known that the physical and chemical stability, the electron mobility and mechanical strength are very high. In addition, the flexibility of graphene is also known as the most promising candidate in the flexible display industry. Therefore, the interest in the unique graphene and new product is dramatically

increased which is a two-dimensional material with superior thermal conductivity using cellulose as a matrix.

These excellent green plastic TIMs which is produced in cellulose and graphene with the overall characteristics of the connector, it can be shown semiconductor and a high value in other to have high-performance thermal management devices. Through various manufacturing processes, studies on film-typed TIMs fabrication are actively carried out using such excellent properties of cellulose and graphene [49]. However, despite the superior properties of such cellulose-based graphene TIMs, the conventional manufacturing process is based on chemical manufacturing methods such as hot pressing, vacuum filtration process, and layered by the layered assembly. It has the disadvantage that not only chemical treatment is required but also extremely high temperature and pressure. Also, these fabrication methods are caused high energy consumption, complicated processes, time-consuming, and it is difficult to make large area TIMs [17].

In this regard, the cellulose-based graphene TIM fabricated using easy, simple and scalable ink coating process is widely expected to be accepted as being used for fabricating the lateral heat spreader [19]. Especially, this ideal thermally conductive paper has excellent thermal conductivity as well as having flexibility, light-weight, and low-cost characteristics. In this regard, the ink coating process for fabricating cellulose-based graphene TIM applied conductive graphene paste, water-dispersible graphene (WDG, hereafter) on the surface of paper substrates are considered [18]. Firstly, paper has the advantages that it can be easily obtained in the surroundings and can be deformed the shape freely according to the targeted system. Also, it is good for having flexibility, absorbing the filler very well as for the porous structure and mechanical properties for not cause plastic deformation. Also, by using the ink coating process, it is possible to fabricate very thin and scalable TIMs. In this regard the purpose of this study for fabricating the cellulose-based graphene TIMs via ink coating process is as follows. First, Instead of existing chemical processes, it is possible to fabricate cellulose-based graphene TIMs using easy and simple ink coating process that can make a scalable TIM [21]. Secondly, the various commercially-available types of paper were considered for fabricating TIMs and investigated its characteristics in respect to the thermal performance of TIMs [31]. And then, characterization of its thermal performance, electrical, and mechanical properties was investigated [20]. Also, the mass fraction of graphene filler and coating thickness was investigated for the effect on the thermal conductivities for the TIMs. Finally, the results of the measured electrical and mechanical properties, clarifying whether its characteristics of the fabricated TIMs are sufficient for using as TIMs for electronic components and thermal management systems.

2. Fabrication

2.1. Types of paper

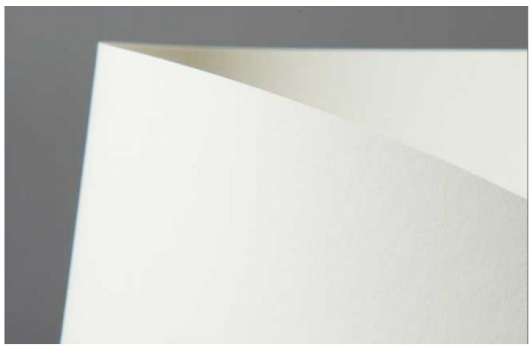

(a)

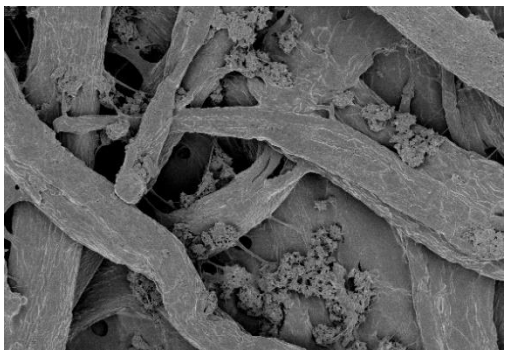

(b)

(c)

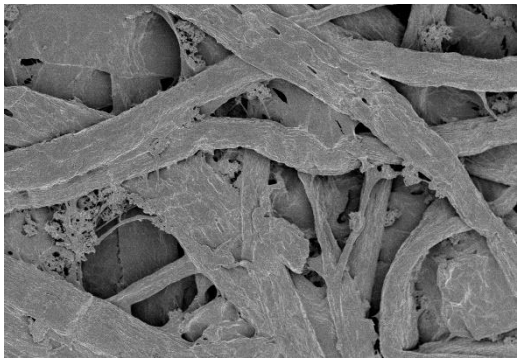

(d)

Figure 2.1. Illustration of (a) image of Munken, (b) SEM images of Munken, (c) image of Matt, and (d) SEM images of Matt

In this study, various types of commercially-available papers are used as matrix materials. Firstly, papers can be easily obtained from surroundings, deform the shape for the use of purpose, has very high flexibility, and has also good mechanical properties that do not occur plastic deformation. Also, there is an advantage that filler can absorb filler well with having the porous structure. And, the paper has many superior properties such as lightweight, low cost, thin, scalable, biodegradability and eco-friendly. Also, by using the ink coating process on the papers, it is possible to fabricate a thin and scalable TIMs in a simple and easy process.

Figure 2.1. show the surface characteristics and the roughness for the SEM images of two types of paper, Munken and Matt. It can be confirmed that Munken shows a rougher surface and much pores between cellulose fibers. On the other hands, in the case of the Matt, it has the smoother surface and the voids between the cellulose have been filled as for the chemical treatment of the surface. In this regard, TIMs were fabricated for the two types of paper in order that considering characteristics such as surface roughness and thickness of each paper to affect the performance of TIMs.

Table 2.1. List of tested as-received papers

Paper	Basis weight [g/m^2]	Thickness [mm]
Bulgyeong	40	0.07
Daerye	85	0.13
Merit	90	0.1
Aqua satin	128	0.12
Wool paper	128	0.18
New craft board	161	0.2

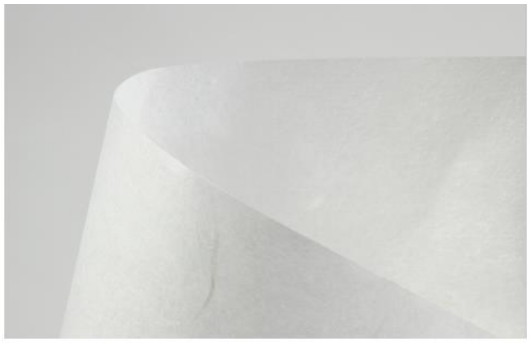

(a)

(b)

(c)

(d)

(e)

(f)

Figure 2.2. Images of tested as-received six types of commercially-available papers of (a) Bulgyeong, (b) Daerye, (c) Merit, (d) Aqua satin, (e) Wool paper, and (f) New craft board.

(a)

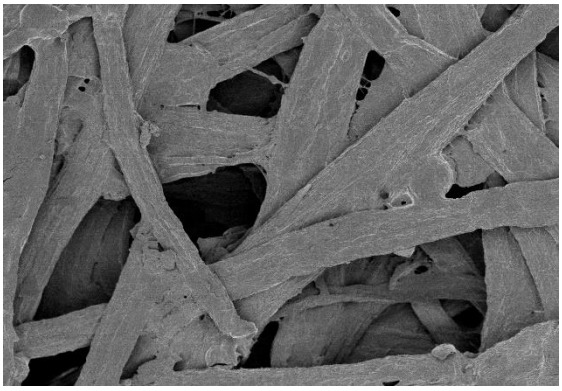

(b)

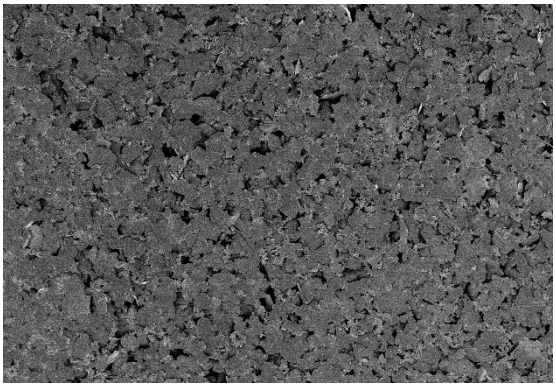

(c)

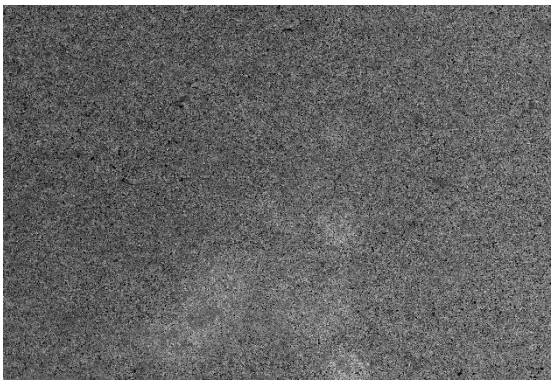

(d)

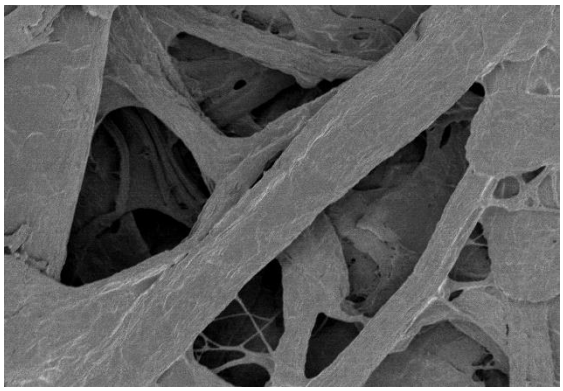

(e)

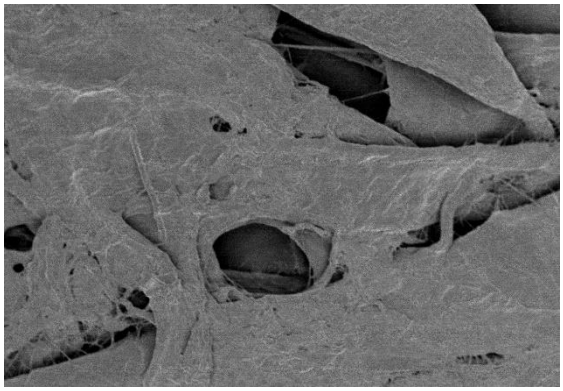

(f)

Figure 2.3. SEM Images of tested as-received six types of commercially-available papers of (a) Bulgyeong, (b) Daerye, (c) Merit, (d) Aqua satin, (e) Wool paper, and (f) New craft board

Also, six types of commercially-available papers: two oriental traditional papers (Bulgyeong and Daerye); merit; aqua satin; wool paper; new craft board are used as matrix materials to fabricate the graphene paper TIMs. The types of papers and their characteristics are showed in the Table 2.1. The figure and SEM images for each paper is shown in Figure 2.2. and 2.3. As with the case of Munken and Matt, their surface characteristics are different. In this regard, the different characteristics of these papers are expected to affect the thermal conductivities of graphene paper TIM [44]. As shown in the SEM images of bulgyeong, daerye, wool paper, and new craft board can see the cellulose fiber which consisting the papers. However, in the case of merit and aqua satin, it can be confirmed that it is chemically surface-treated. Also, it can be confirmed that there are pores between the cellulose fiber for the bulgyeong, daerye, wool paper, and new craft board. This porous structure of papers was expected to absorb graphene filler well and affect the thermal performance of TIMs.

2.2. Dip coating process

Firstly, graphene paper TIMs are fabricated using the dip coating process. Dip coating process show the type of coating process in which a material is immersed in coating solutions or slurry to form a precursor layer on the surface of the material and then baked at an appropriate temperature to obtain a coating film [26]. This process is suitable for processing relatively small products and the surface is uniform and the loss rate of the coating liquid can be reduced. The step of dip coating can be generally classified into five stages. i) Immersion: Dipping the substrate to be coated into the solution of coating material for constant speed of coating. ii) Startup process: The substrate is contained in the coating solution for the appropriate time and then pulled up. iii) Deposition process: A thick layer in the dip

coating process is deposited on the substrate after that the immersed substrate is pulled up. Maintain a constant speed for coating for constant thickness at pull up. This rate determines the thickness of the coating. iv) Drainage: Excessive liquid is discharged from the surface. v) Evaporation: The solvent evaporates and a thin layer is formed. Many factors contributing to determining the final state of thin film dip coating process are contributing. By controlling the number of factors such as initial substrate surface functionality, immersion time, withdrawal rate, number of dipping cycles, solution composition, concentration, temperature, each immersion solution. It is possible to control the thickness of the repetitive various changes in structure and thickness can be fabricated.

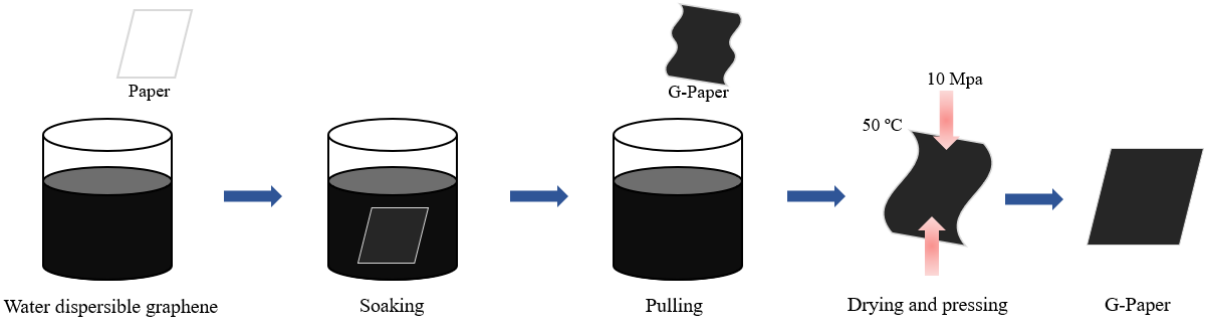

Figure 2.4. Fabrication procedure of graphene-paper-based TIM via dip coating process

Figure 2.4. shows the procedure for fabricating the graphene paper TIMs using the dip coating process. Firstly, TIMs were fabricated using the dip coating process through soaking and pulling the paper in a container containing the WDG. And then, graphene papers without using the co-polymer (G-Paper, hereafter) dries at 50°C for 30 min to evaporate water. Lastly, crimping with 10 MPa will result in a more flatter shape TIM if needed for application of use. In this way, graphene paper TIMs are fabricated by using dip coating process.

The aforementioned coating process is called dip coating process. In this study, another set of sample fabrication is performed to investigate the effect of various coating process. The bar coating and slot die coating process are also used together with the dip coating process. The thermal performances of the graphene paper TIMs are fabricated by those three coating methods are compared later.

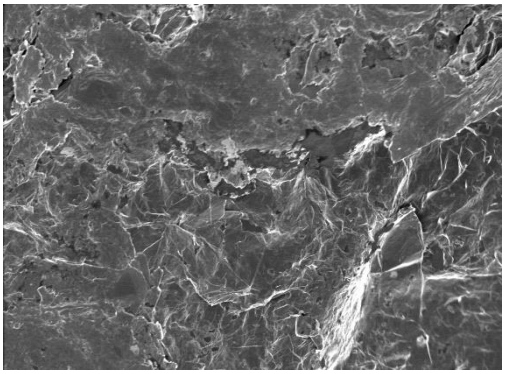

(a)

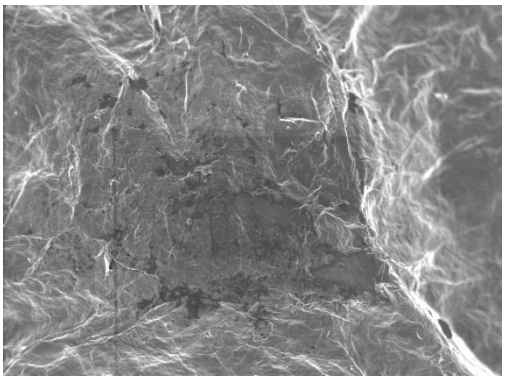

(b)

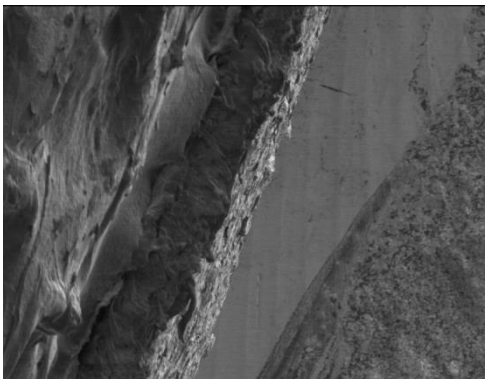

(c)

Figure 2.5. SEM images of the fabricated TIM via dip coating process of (a) Munken, (b) Matt, and (c) Cross-sectional of Matt

Figure 2.5. shows the SEM images of the graphene-paper-based TIMs fabricated by the dip coating process. It can be confirmed that the coating surface is partially imperfect for the both Munken and Matt. And, The WDG solution flows downward effected on the gravity during the soaking and

pulling procedure. As a result, the cross-sectional image of matt shows that the coating thickness is not uniform. Also, TIM fabricated by using the dip coating process is wrinkling [45].

2.3. Use of co-polymer

In order to prevent wrinkling of TIMs fabricated by the dip coating process, the co-polymer having three reactors of polyvinyl acetate (VAc, hereafter), polyvinyl alcohol (VA hereafter), and polyvinyl butyral (VB, hereafter) is used [21]. This co-polymer is often used for the adhesive layer in the coating process and has its own hardness [43]. Also, the copolymer has an advantage of increasing the mechanical strength. It is intended to utilize VB used for engineering plastic with good stability against friction and heat and supplementation itself of the low softening point of the paper itself increases the mechanical strength with the hardening. VA is needed to convert this VB, and VAc is the starting material. It is made to convert from VAc, and the substance remains in the process of conversion to form co-polymer. As a result, the co-polymer affects a structure with good mechanical properties and adhesion.

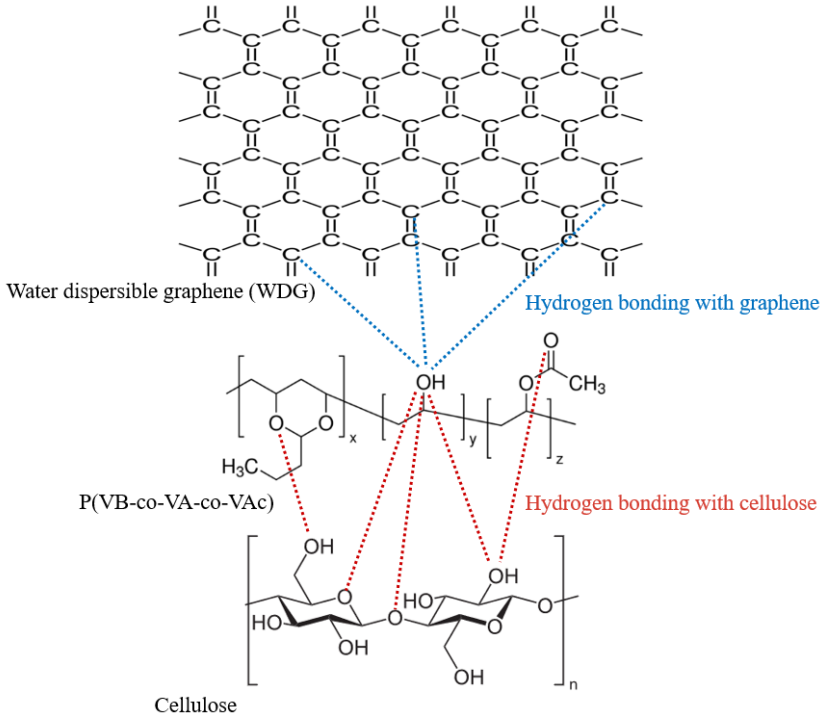

Figure 2.6. Molecular interactions in the formation of between the graphene-paper-based TIMs

As shown in the figure 2.6., this co-polymer has oxygen functional groups such as -O- and -OH- which leads to a strong hydrogen bond between cellulose and graphene to enhance its adhesion. Also, hydroxyl of polyvinyl alcohol such as -OH- binds to the carbon of graphene and increases mutual interaction. The VB provides excellent mechanical strength and bonding properties, resulted that mechanically stable and robust graphene-paper-based TIM. Also, the VAc provides adhesion properties of bonding layer which have the advantages of enhancement for the adhesive interaction between the cellulose and graphene, respectively so that preventing the delamination in adhesion of graphene layer from the copolymer and cellulose matrix. The hydroxyl groups in the VA provided for its compatibility with graphene filler. Because of the improved compatibility between the cellulose, copolymer, and graphene, respectively. it is also possible to be expect for that the graphene-paper using the copolymer will achieve the smooth surface of paper TIMs and better surface morphologies compared with the pristine paper. As for the reduced surface roughness of graphene paper, it is caused that the paper result in better adhesive layer between the cellulose and graphene surfaces in the graphene-paper-based TIMs. As a result, the co-polymer is used to prevent the wrinkling and enhance the mechanical strength of the graphene paper TIMs by increasing the adhesion between cellulose and graphene.

(a)

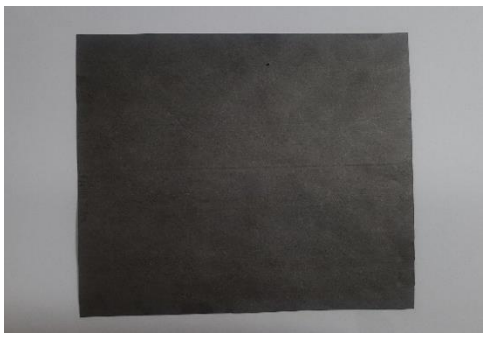

(b)

Figure 2.7. Images of G-Paper and G/P-Paper via bar coating

Figure 2.7. shows the wrinkling of G-Paper for the dip coating process. In the dip coating process, it is difficult to control the coating thickness and reproducibility. And, wrinkling occurs in the fabricated TIMs. Such wrinkling is not only bad for the appearance but also ruins the applicability for practical uses. The result of hydrogen bond between the interactions, the structure of the cellulose matrix brings open states more and allowed the molecules to penetrating into the porous structure of cellulose matrix and affect to the conformation behavior and the volume expansion in the cellulose matrix. On the drying process, the mocules of solvent are removed and such conformation behavior and volume expansion become locked in, usually resulting in the wrinkling effect in the cellulose paper. On the other hands, there are no wrinkling effects on the surface of the graphene-papers. It is attributable to the fact that copolymer brings an important effect of preventing the volume expansions in graphene paper and conformation behavior in the cellulose matrix with the strong hydrogen bond which have interaction with the cellulose, copolymer, and graphene.

2.4. Bar coating process

According to the bar coating process, the thickness of the coated thin film can be adjusted from a few nanometers to hundred micrometers depending on the coating speed and the diameter of the wire wrapping the wire wound rod. Also, the bar coating process has the advantage that the solution used is directly printed on the substrate without waste of solution so that the consumption of the material can be minimized.

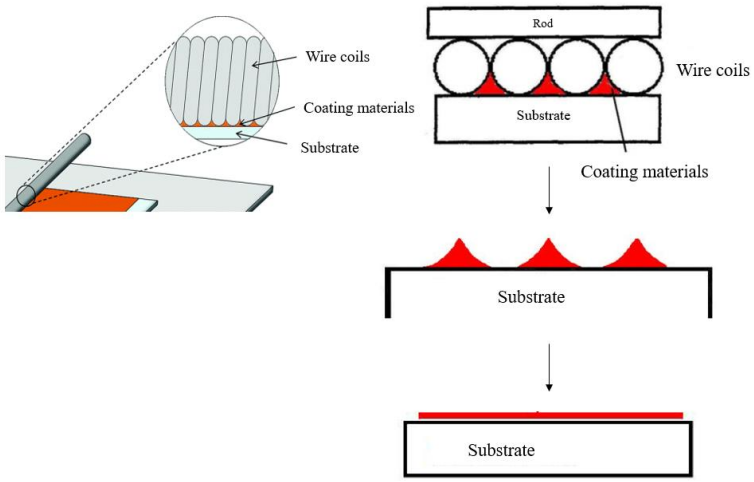

Figure 2.8. Schematic diagram of bar coating process

Figure 2.8. shows the principle of bar coating process. Slide the solution horizontally using a coating bar on which a wire of several tens of micro diameter is wound and apply it on the substrate. The solution is filled between the wound wire and this amount the concentration of the solution directly affect the thickness and quality of the film. The bar coating process can be a scalable process, shortening the manufacturing time, as well as using a very easy and simple process. The bar coating processes are as follows. i) Coating solution is evaporated in front of the wire wound rod coating bar, ii) Wet coating of substrate coating solution horizontally by movement of wire load bar along the substrate. iii) Gradually dry the wetted film from the ends of the substrate to the center. The groove between the coil of the wire wound around the bar determines the amount and thickness of coating solution that passes as it travels along the substrates [30]. That is, the thickness of the coating is determined by the amount of the coating solution depending on the diameter of the rod, the viscosity of the solvent, the surface tension, the surface energy of the substrate, the surface roughness of the substrate, and the coating speed of wire wound rod. When choosing the wire rod size of coil, the ratio of coating thickness of wetted film to the wire diameter is generally 1:10. Also, the bar coating process provides excellent film homogeneity, smooth surface for a large area hardened or flexible substrate. Therefore, in the bar coating process it is possible to fabricate thin and scalable graphene paper TIMs for uniform coating surface and thickness.

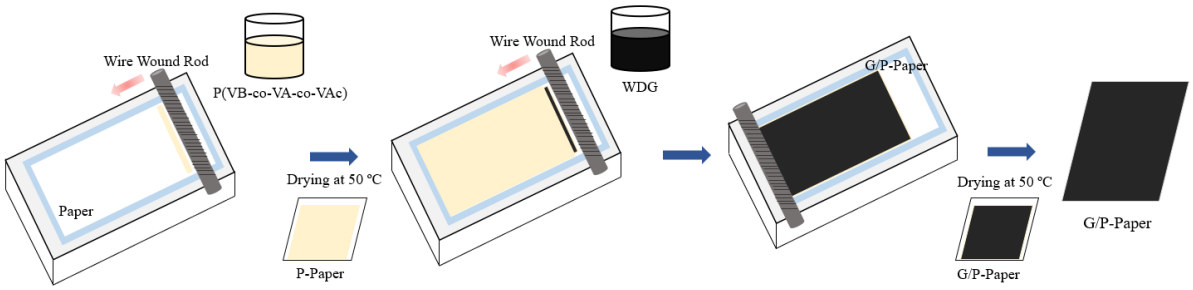

Figure 2.9. Fabrication procedure for graphene-paper-based TIM via bar coating process

Figure 2.9. shows the procedure for fabricating graphene paper TIMs using a bar coating process. Firstly, P(VB-co-VA-co-VAc) copolymer solution mixed ethanol: copolymer = 80: 20 by the mass fraction is coated on a selected paper using the Meyer Rod & Air knife Coater followed by drying at 50ºC for 15 min. As an adhesion layer, the paper is treated with copolymer, before the deposition of graphene solution. This copolymer layer provides a high adhesion layer for heat transfer and the robust structure mechanically. To achieve graphene papers TIMs, WDG (MExplorer Co. Ltd) paste is used as

an active material. The density of the used WDG is 25 mg/mL. Then, the WDG is coated again on the paper coated with co-polymer and dried using the same coting process. The G/P-paper is dried at 50°C for 30 min to evaporate water.

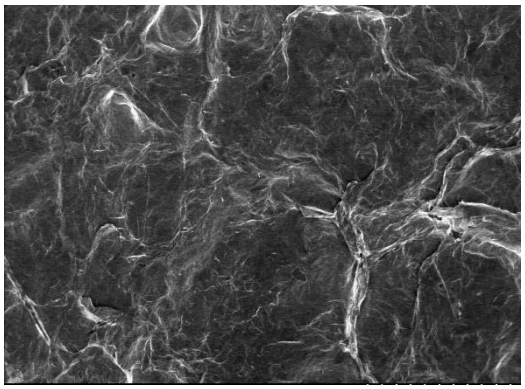

(a)

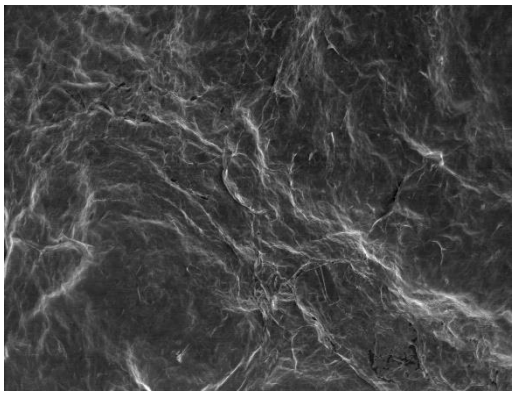

(b)

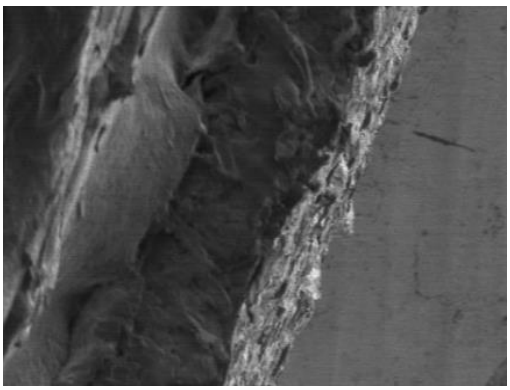

(c)

Figure 2.10. SEM images of fabricated TIMs via bar coating process of (a) Munken, (b) Matt, and (c) Cross-sectional of Matt

Figure 2.10. shows the SEM images for graphene paper TIMs fabricated using the bar coating process. It is possible to know that the coating thickness is almost constant. Also, it can be confirmed that the nearly uniform coating thickness through the cross-sectional SEM images.

2.5. Slot die coating process

The slot die coating process that is the pre-metered process whose the thickness of coating is adjusted for the flow meter, slides liquid fluids such as slurry, adhesive, hard coating agent, and ceramics having flow by a pulsating pump or a piston pump called Rheology [38]. It designed inside the mold supplied between the upper and lower mold plates and supplied fluid from the liquid supply pipe to the fabric, film, glass version, uniform in thickness in the width direction of the sheet traveling direction followed by coating. The slot die coating process has no exposure of liquid form liquid tank to slot die and there is no viscosity change of the material and coating is possible. In addition, since the coating is carried out using a metering pump, it is a sealing process which enables a certain amount of coating to be performed and which can be excellently controlled with highly precise weighing process technology. The coating thickness can be easily controlled and stabile reproducibility of the coating are good. The thickness of the coating is influenced by flow velocity, operation interval, film thickness, web speed, die setting, and liquid physical properties.

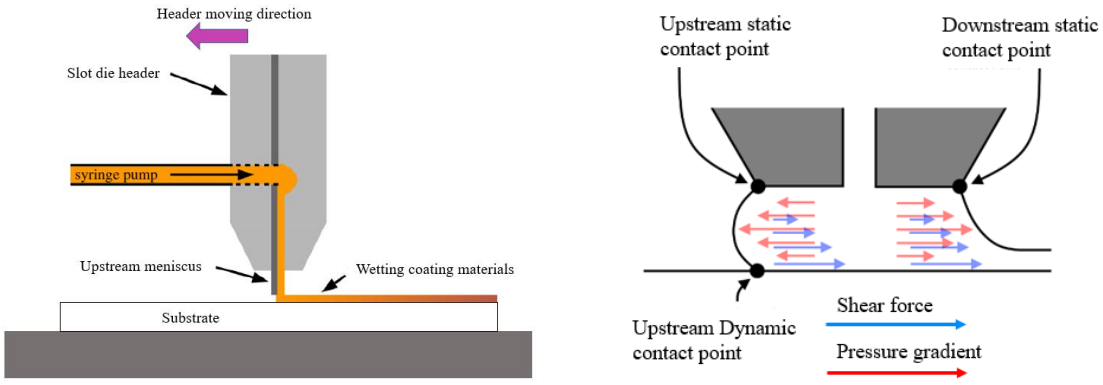

Figure 2.11. Schematic diagram of slot die coating process

Also, as shown in figure 2.11., in order to obtain the uniform coating thickness, the coating gap between the slot die header and the substrate is set. And then, unlike bar coating which applies to coat after solution, the solution is applied and coated so that more precise coating thickness control is possible. Also, it is fabricated for the large area of TIM.

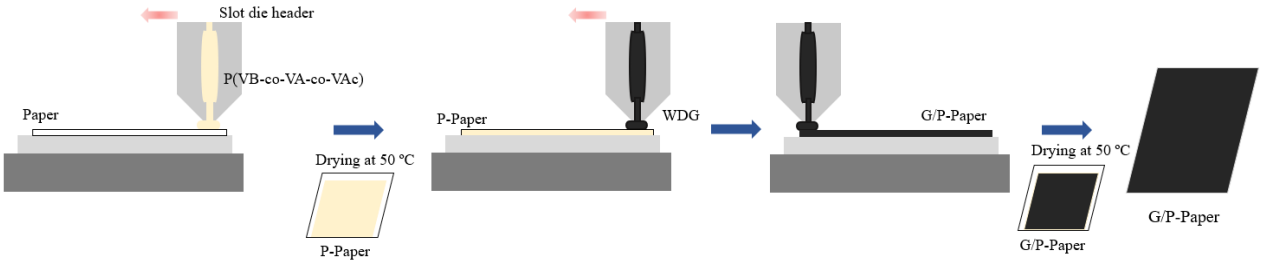

Figure 2.12. Fabrication procedure for graphene-paper-based TIM via slot die coating process

As shown figure 2.12., the slot die coating process for fabricating graphene paper TIMs are as follows. The first step, Adjusting selected paper on the substrate for coating the copolymer solution using slot die coater and then dry it at 50ºC for 15 min. Then, after setting the desired thickness on the coordinate axis and then coated the WDG again on the P-Paper using the slot die coater [25]. Finally, it is dried again at 50ºC for 30 min. As a result, the graphene paper TIMs fabricated by using slot die coating process is fabricated.

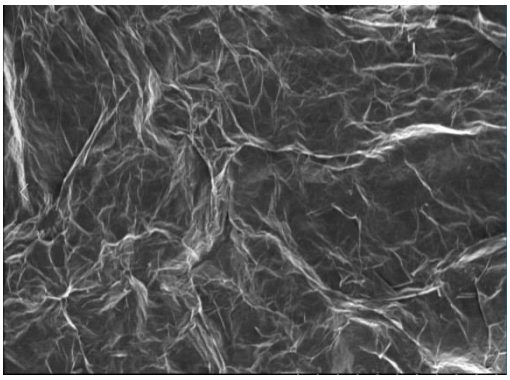

(a)

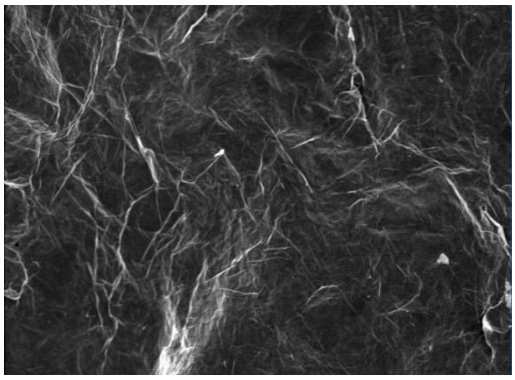

(b)

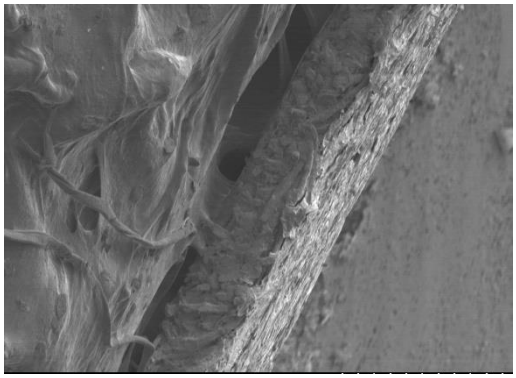

(c)

Figure 2.13. SEM images of fabricated TIM via slot die coating process of (a) Munken, (b) matt, (c) cross-sectional of Matt

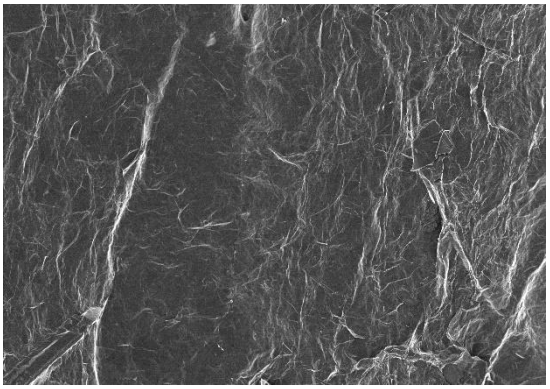

(a)

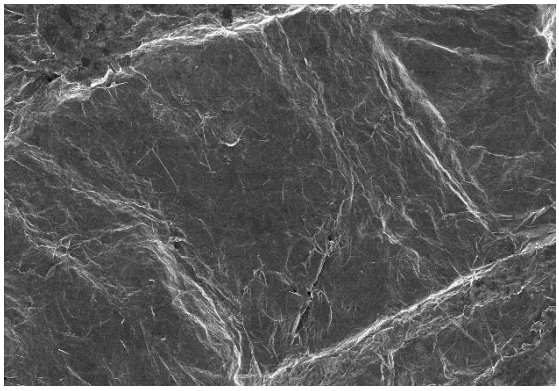

(b)

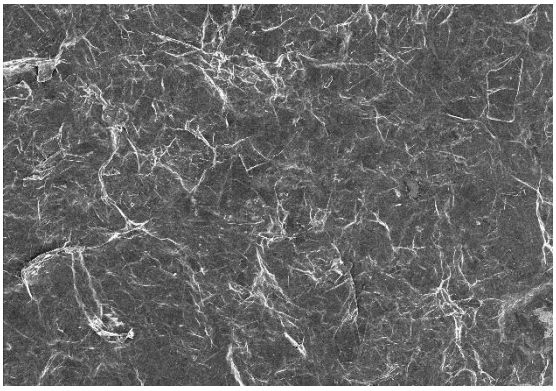

(c)

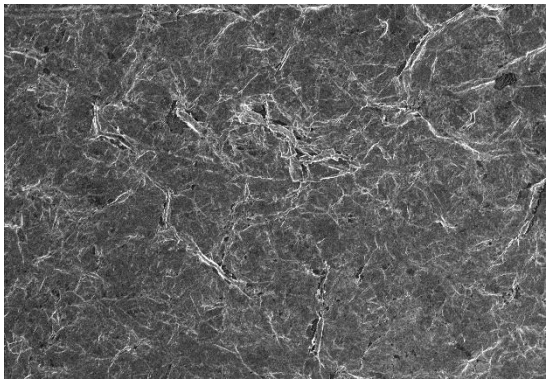

(d)

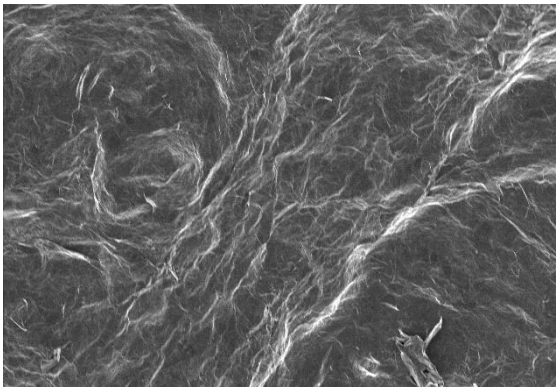

(e)

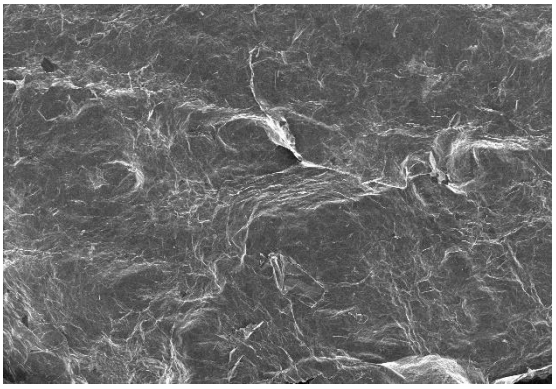

(f)

Figure 2.14. SEM images of fabricated TIM via slot die coating process of (a) Bulgyeong, (b) Daerye, (c) Merit, (d) Aqua satin, (e) Wool paper, and (f) New craft board

Figure 2.14. show the surface coating and the cross-sectional SEM images of graphene paper TIM fabricated using slot die coating process. It is confirmed that it is possible to control the uniform surface coating state and the coating thickness more precisely than dip coating and bar coating process. In this way, graphene paper TIMs are fabricated easy, simple, and scalable process using the dip coating, the bar coating and the slot die coating process.

3. Experimental method

3.1. Laser Flash Analysis

In this study, the thermophysical properties of the fabricated graphene paper TIMs are measured at 25°C using Laser Flash Analysis (LFM, hereafter). In this study, XFA 300, LINSEIS Inc. was used for the LFM. In the laser flash technique, the thermal diffusion coefficient (α) is directly measured and the thermal conductivity is calculated by multiplying the thermal diffusivity (α), specific heat (C_P), and density (ρ) [12].

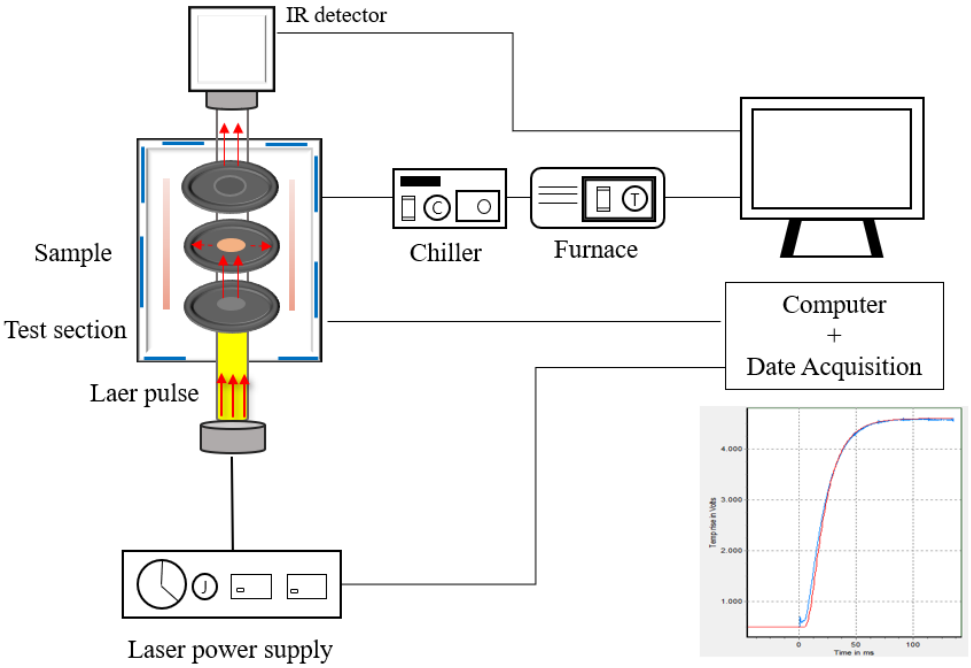

Figure 3.1. The schematic diagram of Laser Flash Method

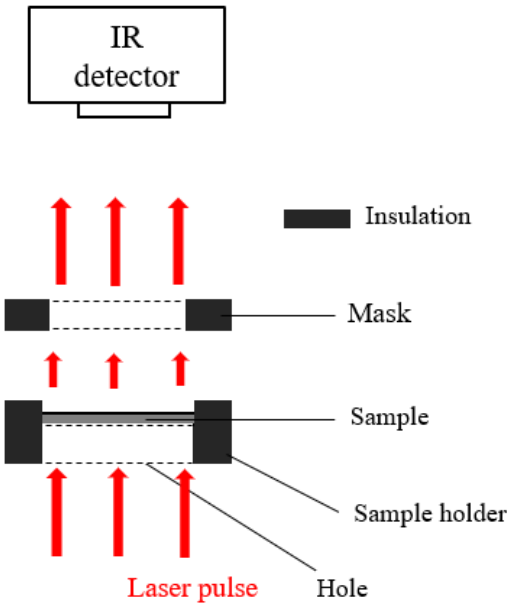

(a)

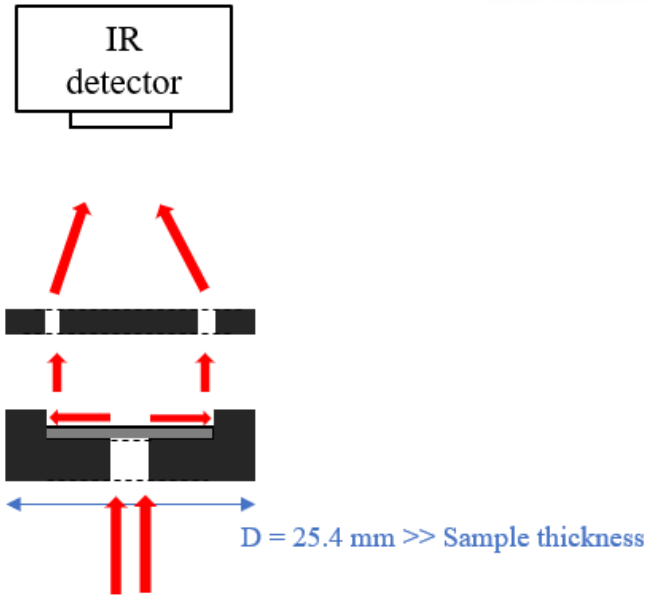

(b)

Figure 3.2. Schematic illustration of (a) through-plane holder and (b) in-plane holder

The principle of the LFM is shown in the Figure 3.1. The Laser Flash Technique uses a xenon flash lamp to investigate thermal conductivity [39]. The tested sample is placed on the test section. The laser pulse on the front surface (x=0) of the sample, a laser pulse is applied to provide a uniform heat flux. And, the absorbed thermal energy at this time is transmitted to the backside of the test object. Temperature rise on the opposite surface reaches a maximum temperature for the time measured by the nitrogen cooled IR sensor as depending on the measuring time. Both top and bottom surfaces of the sample is coated with graphite powder to ensure uniform heat flow and thermal diffusion. In addition, it is possible to measure under desired temperature conditions via furnace and these controls are done through the computer software.

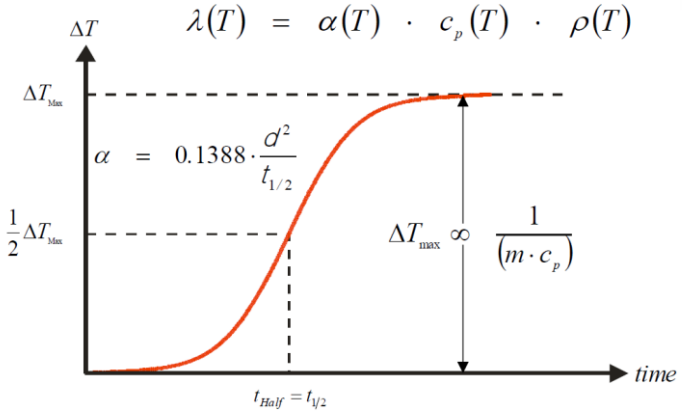

Figure 3.3. Temperature rise on the rear surface of sample over time

In this regard, the thermal diffusivity can be extracted from the analysis of measured temperature curve over time as shown in figure 3.2. Developed by Parker, the thermal diffusion measurement method by laser flash technique has also been proposed. The temperature distribution at the midpoint to the rear surface of the sample can be expressed as a function of the thickness L of the sample and the time t as

$$T(L,t) = T_{\max}\left(1+2\sum_{n=1}^{\infty}(-1)^n \cdot e^{-\frac{n^2\pi^2\alpha t}{L^2}}\right)$$

Where $T_{\max}$ is the maximum temperature of the midpoint of rear surface, which corresponds to the steady-state temperature caused by the laser pulse. In the LFM, the time required for halfway increase of temperature compared with the maximum temperature with reference to the initial temperature, namely the 'half time' ($t_{1/2}$) is measure.

$$T(L,t) = 0.5T_{\max}$$

The relational expression obtained by converting the thermal diffusion at the point where the temperature of the back surface of the test piece reaches 1/2 of the maximum rising temperature ($t_{1/2}$) is as

$$\frac{1}{2} \approx \left(1-2e^{-\frac{\pi^2\alpha t_{1/2}}{L^2}}\right)+\left(1+2e^{-\frac{4\pi^2\alpha t_{1/2}}{L^2}}\right)+\left(1-2e^{-\frac{9\pi^2\alpha t_{1/2}}{L^2}}\right)+\cdots$$

Finally, the thermal diffusivity alpha is determined the following approximated correlation by the sample thickness and the time when it takes to reach the half of the maximum temperature is as

$$\alpha \cong 0.13879 \frac{L^2}{t_{1/2}}$$

Measurement of half time based on LFM directly yields the value of thermal diffusivity as shown in the above equation. In order to estimate the thermal conductivity from the measured thermal diffusivity, the density and the specific heat of sample should be obtained according to the following definition of thermal diffusivity.

$$\alpha = \frac{k}{\rho c_p}$$

The specific heat of the sample can be also measured from the LFA technique via comparison with the temperature rise of the sample with reference sample with the same input energy of laser pulse experimental conditions named coating method as shown in figure 3.3.

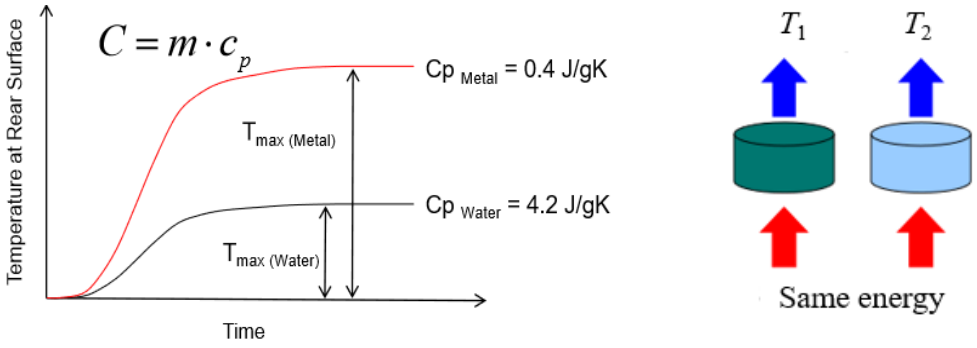

Figure 3.4. The principle of measuring the specific heat

The specific heat of the substance can be expressed as the following equations.

$$C_p = \frac{Q}{\rho L \Delta T}$$

Through the comparative sample whose density, thickness, and specific heat value are known. For a given energy input Q, the temperature rise of a sample is obtained given as the following equations:

$$Q\varepsilon = \rho L C_p \Delta T$$

Where ε, ρ, L, C_p, and ΔT represents emissivity, density, thickness, specific heat, and temperature rise, respectively. The equation also can be applied to the reference sample as follows:

$$Q\varepsilon' = \rho' L' C_p' \Delta T'$$

The superscript' denotes the property of the comparative sample. The both surface of the tested sample is coated for the material of the comparative sample prior to the test to set the emissivity of the tested sample as the same value with the reference sample, thus, ε is equal to ε'. Therefore, the specific heat of the unknown sample is as

$$C_p = \frac{\rho' L' \Delta T' C_p'}{\rho L \Delta T}$$

The density of the sample is calculated by estimating the mass, calculating the volume and then dividing the mass into volumes. Also, the thickness of the sample is measured using a digital micrometer. The accuracy of the laser flash technique measurement using LINSEIS XFA 300 Xenon flash instrument is about ~ 5 %.

3.2. Four-points probes measurement method

The four-points probes (FPP, hereafter) method developed by Valdes is most widely used to measure sheet resistance or resistivity of thin films and semiconductor materials. The main techniques for measuring sheet resistance are collinear the four probes are brought into contact with the surface of the sample. The resistance is measured by the four-points probes method and the sheet resistance is measured by applying the geometric correction coefficient. These sheet resistance or sheet resistivity are common electrical characteristics used for evaluating the properties of thin films of conductivity and semiconductor material. Compared to other resistance measurements, the main advantage of sheet resistance is irrelevant to the size of the rectangle. So, comparison of electrical properties between other samples is easy. Another advantage could be directly measured using FPP.

Sheet resistance is generally defined as the resistance of a material divided by the thickness. Such sheet resistance units are commonly used in ohm/square. The sheet resistance is a measure of the resistivity of a thin film sample that are nominally uniform in thickness. In a regular three-dimensional conductor, resistance is as follows:

$$R = \rho \frac{L}{A} = \rho \frac{L}{Wt}$$

The sheet resistance can be expressed resistivity divided by the thickness of the sample as follows:

$$R = \frac{\rho}{t} \frac{L}{W} = R_S \frac{L}{W}$$

The four-points probes consist of four electrical probes on the top and maintain the same spacing. Apply current to the external two probes and operate by measuring the voltage drop between the two internal probes.

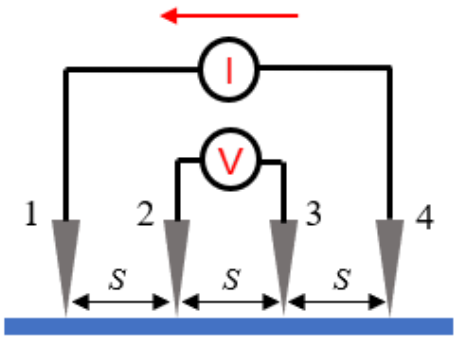

Figure 3.5. Configuration of 4-probe-measurement method

Sheet resistance can be obtained by using the following equation as shown in the figure 3.4. For the bulk sample which is thickness is much larger than spacing of probe, a spherical current ring from the outer probe tips can be assumed as follows

$$\Delta R = \rho \frac{dx}{A}$$

Where ρ is the resistivity, dx is the differential length, and A is the surface area penetrated by the current from one probe. In this regard, for determining the resistance between the voltage measurement tips, one integrates between x_1 and x_2 is as

$$R = \int_{x_1}^{x_2} \rho \frac{dx}{2\pi x t} = \int_{s}^{2s} \rho \frac{dx}{2\pi x t} = \frac{\rho}{2\pi t}(\ln x)\Big|_{s}^{2s} = \frac{\rho}{2\pi t}\ln 2$$

Superposition of current at outer two tips leads to R=V/2I, so that

$$\rho = 2\pi s(\mathrm{V/I})$$

For a thin film sample which is thickness is less than probe spacing, it is assumed that the case of current rings

$$\rho = \frac{\pi t}{\ln 2} 2R = \frac{\pi t}{\ln 2} 2\left(\frac{\mathrm{V}}{2\mathrm{I}}\right) = \frac{\pi t}{\ln 2}\frac{\mathrm{V}}{\mathrm{I}}$$

As before, superposition of current at the outer probe two tips leads to R=V/2I, so that the sheet resistance for a thin film sample is as, is not dependent on the probe spacing.

$$R_S = \frac{\rho}{t} = \frac{\pi}{\ln 2}\frac{\mathrm{V}}{\mathrm{I}} = 4.53\frac{\mathrm{V}}{\mathrm{I}}$$

Here, constant is a geometric factor and in the case of thin film taht is for a semi-infinite is 4.53.

This equation are valid for the material being tested is not thicker than 40 % of the gap between the probes, very thin layer thickness t << probe spacing s, and it should be noted that width of the sample is sufficiently large.

4. Results and discussion

4.1. Thermal conductivity

The thermal conductivities of the fabricated graphene paper TIMs is measured at 25 °C using the LFM, laser flash technique, previously described [19]. The measured thermal conductivities according to types of coating process and papers are as follows.

Table 4.1. Effect of coating process on the thermal conductivities

Coating process	Paper	Thickness [mm]	In-plane thermal conductivity [W/m-K]	Through-plane thermal conductivity [W/m-K]
None	-	0.1	~ 0.05	~ 0.05
Dip coating	Munken	0.18	3.26 ± 0.2	0.09 ± 0.01
Dip coating	Matt	0.17	3.03 ± 0.23	0.08 ± 0.01
Bar coating	Munken	0.13	5.75 ± 0.36	0.11 ± 0.01
Bar coating	Matt	0.13	5.65 ± 0.37	0.09 ± 0.01
Slot die coating	Munken	0.13	6.05 ± 0.35	0.12 ± 0.01
Slot die coating	Matt	0.13	5.89 ± 0.37	0.11 ± 0.02

Table 4.1. summarizes the effect of the coating process on the in-plane and through-plane thermal conductivity of the graphene paper TIMs. In this table, the paper type is fixed as the Munken and Matt which are the commonest type among commercially-available papers. The thermal properties of the as-received pristine papers are ~ 0.05 W/m-K. By applying the coating of copolymer and graphene, the thickness of the papers are increased by 30-80 %. It has been confirmed that the thermal conductivity of the pristine paper is significantly enhanced by the amount of 100 times by coating the graphene. The slot die coating process resulted in the largest in-plane thermal conductivity ~ 8 W/m-K, while the dip coating showed the worst performance. In addition, the slot die coating provides the lowest and even thickness. Therefore, the slot die coating was chosen as the fabrication process of the graphene paper TIMs in this study. It can be confirmed that in-plane thermal conductivities are much higher than the through-plane thermal conductivities. This is due to the weak cohesion force of cellulose and graphene in the through-plane direction, as indicated by many previous studies. The slot die coating showed the largest through-plane thermal conductivity among the three coating processes.

As for the effect on the coating thickness for the coating process, it is found that the thicknes s is much thicker in case of the dip coating process. In the case of the bar coating and slot die coating process, it is possible to fabricate the thin TIMs. In case of the dip coating process, the results of the m easured thermal performance show that the in-plane thermal conductivities are 3.26 W/m-K and 3.03 W/m-K and the through-plane thermal conductivities are 0.09 W/m-K and 0.08 W/m-K for Munken and Matt, respectively. For the bar coating process, it shows that the in-plane the rmal conductivities are 5.75 W/m-K and 5.65 W/m-K and the through-plane thermal conductivit ies are 0.11 W/m-K and 0.09 W/m-K for the Munken and Matt, respectively. In case of the slot die coating process, in-plane thermal conductivities show 6.05 W/m-K and 5.89 W/m-K and the through-plane thermal conductivities are 0.12 W/m-K and 0.12 W/m-K for the Munk en and Matt, respectively [25].

Through the measured results of thermal conductivity, it is shown that the thickness of graphene paper TIM is the largest in the case of dip coating process. However, the thermal conductivity is the worst. Especially, for the in-plane thermal conductivity, the differences are larger than through-plane thermal conductivity. As for the bar coating and slot die coating process, it was found that they show similar thermal conductivity for both the in-plane and through-plane regardless types of paper. It can be assumed that the role of copolymer affects the thermal performance of fabricated TIMs as a measurement result. Also, the bar coating and slot die coating processes, the thermal conductivities affected by only the graphene coating thickness. It also shows the in-plane thermal conductivity are much higher than the through-plane thermal conductivities.

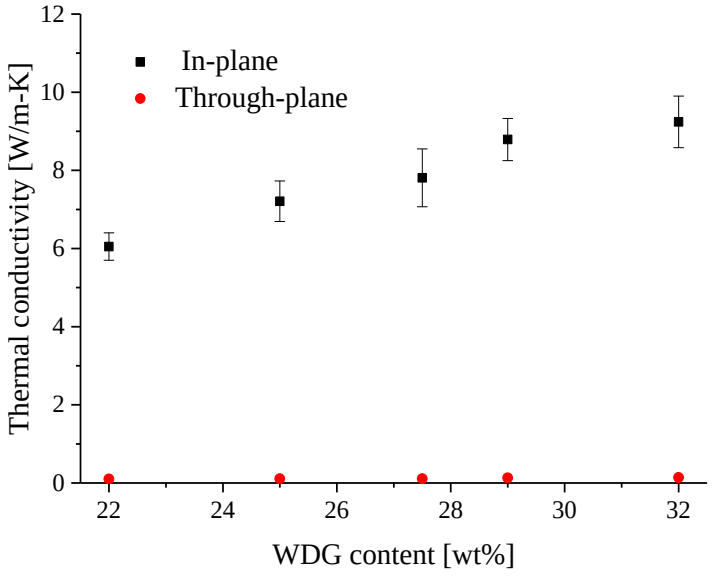

(b)

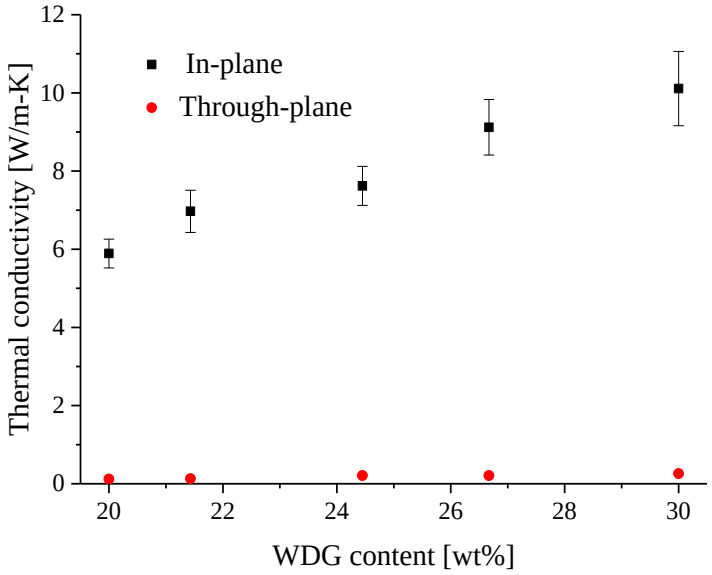

(b)

Figure 4.1. Effect of WDG content on the thermal conductivities of (a) Munken and (b) Matt

Figure 4.1. shows the effect of WDG content by weight on the in-plane and through-plane thermal conductivities [27]. As shown in this figure, the in-plane thermal conductivity a

lmost linearly improves with the WDG contents [48]. In case of Munken containing the WD G contents are from the mass fraction of 22 wt.% to 32 wt.%, in-plane thermal conductivities increase from 6.05 W/m-K to 9.24 W/m-K and the through plane thermal conductivities incre ase from 0.1 W/m-K to 0.14 W/m-K. In case of matt containing the mass fraction of WDG contents varies from 20 wt.% to 30 wt%, the in-plane thermal conductivity improves from 5.89 W/m-K to 10.11 W/m-K. Also, through-plane thermal conductivity increase from 0.12 W/m-K to 0.26 W/m-K at the same mass fraction contents.

It can be confirmed that increasing the mass fraction of the WDG affect the higher thermal conductivities for both in-plane and through-plane [31]. Also, the in-plane thermal conductivity almost linearly increases with the WDG contents. This is due to the fact that the increasing as a conductive filler which affects the thermal conductivities of TIMs as the amount of WDG contents are increased.

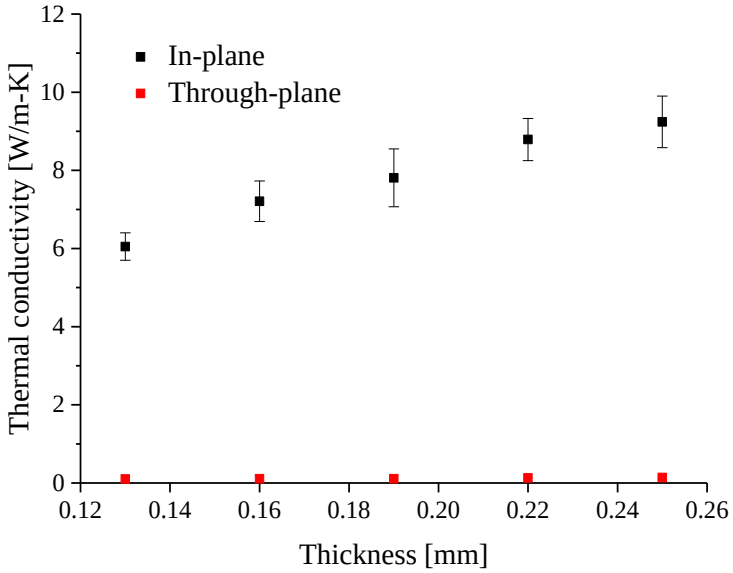

(a)

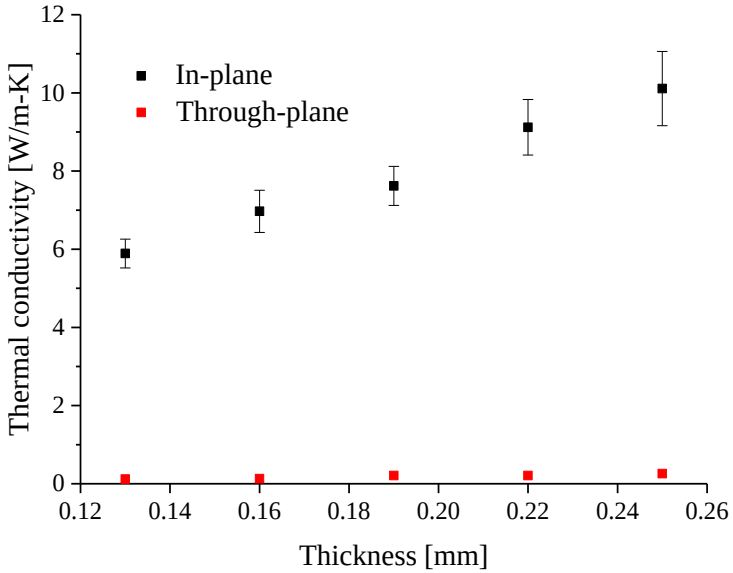

(b)

Figure 4.2. Effect of thickness content on the thermal conductivities of (a) Munken and (b) Matt

Also, the thickness of graphene layers increases in proportion to the WDG contents, as verified Figure 4.2. The thermal conductivities are also investigated according to the coating thickness which is an important factor of film-typed TIM [35]. Regardless of the type of paper, it can be confirmed that the thermal conductivities increase as the coating thickness both in the in-plane and through-plane thermal conductivity. In the case of Munken, the in-plane thermal conductivity varies from 6.05 W/m-K to 9.24 W/m-K and the through-plane thermal conductivity varies from 0.1 W/m-K to 0.14 W/m-K depending on the thickness variation from 0.13 mm to 0.25 mm. For the Matt, as the thickness varies from 0.13 mm to 0.25 mm, the in-plane and through-plane thermal conductivity improves from 5.89 W/m-K to 10.11 W/m-K and 0.12 W/m-K to 0.26 W/m-K for the variation of thickness respectively. As with the mass fraction, this is due to an increase in the amount of WDG paste affected the thermal conductivity. This figure also shows that the in-plane thermal conductivity also linearly increases with the measured coating thickness. Furthermore, the increase of the in-plane thermal conductivity is much greater than the tendency for the through-plane thermal conductivity. The through-plane thermal conductivity is shown to be not significantly affected by the WDG content or coating thickness. The anisotropic thermal conductivities of graphene paper TIM considered in this study are due to the crystal structure of graphene which acts as a conductive fillers. Therefore, it is necessary to select an appropriate TIMs haivng high thermal conductivities as satisfying the conditions of the thickness for thermal management application.

4.2. Effect of paper types

Table 4.2. Effect of paper types on the thermal conductivities

Paper	Thickness [mm]	In-plane thermal conductivity [W/m-K]	Through-plane thermal conductivity [W/m-K]
Bulgyeong	0.1	6.78 ± 0.53	0.16 ± 0.02
Daerye	0.16	6.32 ± 0.41	0.14 ± 0.01
Merit	0.13	4.82 ± 0.41	0.12 ± 0.02
Aqua satin	0.15	4.35 ± 0.23	0.11 ± 0.02
Wool paper	0.21	5.87 ± 0.53	0.13 ± 0.03
New craft board	0.23	5.71 ± 0.24	0.13 ± 0.02

Table 4.2. shows the effect of the paper types and thickness on both in-plane and through-plane thermal conductivities. It can be confirmed that the thermal conductivities are different according to the paper types, despite the same coating thickness of 3-mm thick [38]. Oriental traditional papers, Bulgyeong and Daerye, and wool paper show relatively high thermal conductivities. As in the previous results, it also shows that the in-plane thermal conductivities are relatively higher than the through-plane thermal conductivities.

In this regard, the porosity of each paper was investigated. Porosity means a measure of void spaces in a material to calculate the volume of void-space divided by total volume of material. The porosity of the paper except for the surface treated merit and aqua satin can be obtained by the following equation.

$$\varepsilon = \frac{V_V}{V_T}$$

Where, ε, V_v, and V_T represesnts porosity, volume of void-space, and total voume of material, respectively.

If the void space is filled with air, the porosity of papers is as

$$\varepsilon = 1 - \frac{\rho_{\text{Bulk}}}{\rho_{\text{Particle}}}$$

Where, ρ_{Bulk} and ρ_{Particel} means the density of paper and cellulose, respectively.

Table 4.3. Basis weight of six-types of paper

Papers	Basis weight [g/m^2]
Bulgyeong	85
Daerye	40
Merit	90
Aqua satin	128
Wool paper	128
New craft board	161

The density of cellulose is 1.5 g/m^3 and the basis weight which means g/m^2 are as table 4.3. Also, the density of paper is obtained basis weight divided by the thickness of each paper. To investigate porosity of surface treated merit and aqua satin, the additives were investigated. In the coated paper, the glossy paper has a pigment less than ~ 20 g/m^2 and is typically art paper. Also, nonglossy paper means paper with pigment of less than ~ 10 g/m^2, aqua satin and matt. Lightweight coated paper is less than ~ 5 g/m^2 of pigment of merit. In this regard, the porosity of merit and aqua satin were obtained by considering the amount of pigment contained in the papers. The pigments used for surface coating of papers consist of clay and ground calcium carbonate (GCC, hereafter). Most of these pigments have a mass fraction of 30 to 70 of clay and GCC. Also, the contained volume of each element is obtained by considering properties of cellulose, clay, and GCC. The contained volume ratio of clay and GCC are less than 3 % in paper. As a result, the porosity of Merit and Aqua satin considering all of the cellulose, clay, and CGG can be obtained as 31.42 % and 41.56 %, respectively.

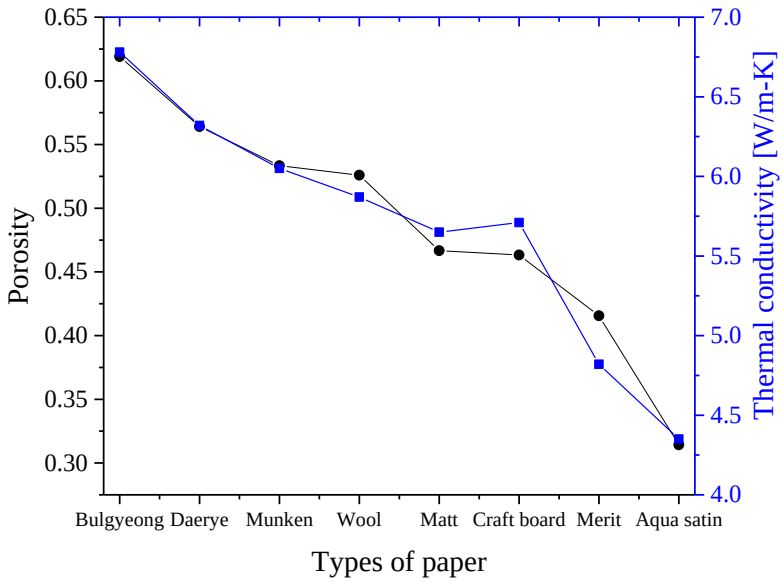

Figure 4.3. Effect of paper types on the thermal conductivities

Figure 4.3 shows the effect of paper types on the in-plane thermal conductivities. The properties of each cellulose are same and additives are negligible other than pigments. As a result, it can be confirmed that the porosity which is characteristics of paper and thermal conductivities are somewhat proportional. It can be assumed that that the paper with high porosity can absorb WDG well and it achieves the enhanced heat transfer path with cellulose. However, most high porosity paper has a disadvantage of low mechanical strength, so it is necessary to select the appropriate paper suitable for the application.

From the measured thermal conductivities, it can be confirmed that in-plane thermal conductivities are significantly remarkable than the through-plane thermal conductivities. This is due to the properties of graphene which plays a role of thermally conductive filler of graphene paper TIMs.

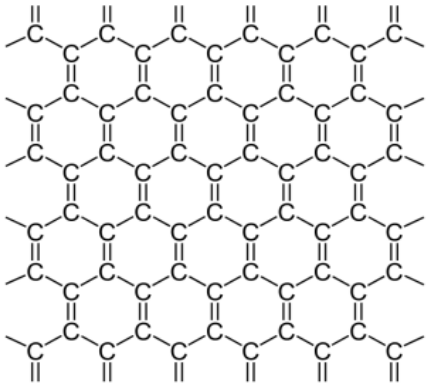

Figure 4.4. Illustration of the crystal structure of graphene

Graphene is one of the carbon allotropes and the crystal structure is in-plane direction of a two-dimensional structure connected to each other in a hexagonal structure with alternating double bonds between carbon atoms as shown in the figure 4.4. [50].

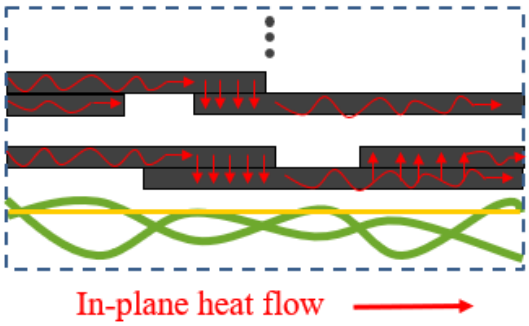

(a)

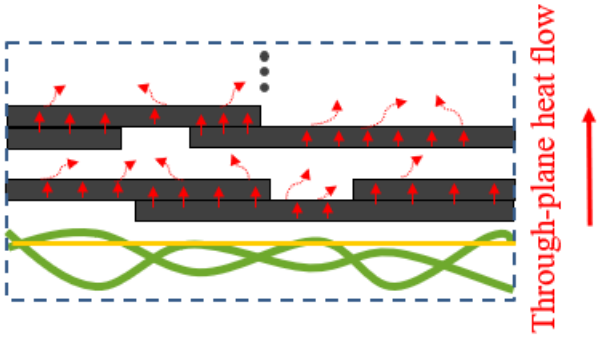

(b)

Figure 4.5. Comparison of heat transfer path of (a) in-plane and (b) through-plane heat flow

In general, thermal conduction occurs when atomic vibrational energy is transmitted. In this regard, graphene has a strong bond extending between the carbon in the plane direction and can transmit the vibration energy more quickly for in-plane direction as shown in the figure 4.5.. Practically used graphene is present in laminated form but the van der Waals forces between the graphene atoms in the vertical direction are weak and the through-plane thermal conductivity is relatively low. In this way, due to the crystal structure of graphene which acts as a conductive filler, highly anisotropic thermal conductivity occurs. The highly anisotropic thermal conductivity of these cellulose-based graphene TIM is useful for thermal management in the form of a thin film for the latest electronic components. However, it should be noted that the limitation through-plane thermal conductivity may be a bottleneck for useful thermal management systems.

4.3. Hybrid filler

The in-plane alignment of graphene in TIMs suppresses the through-plane heat transport [22-24]. It limited the performance of TIMs in geometry normally required for thermal management applications. The utilization of multicomponent fillers which include particles different shapes and dimensions is a common practice in the fabrication of TIMs. In this regard, combining the graphene with other fillers in order to enhance through-plane heat transfer path is studied.

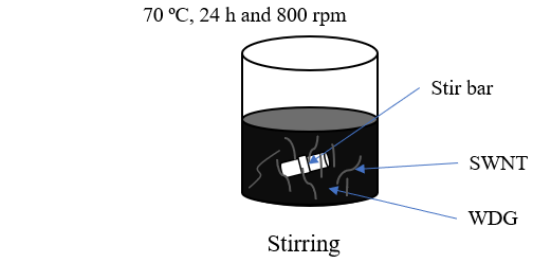

(a)

(b)

Figure 4.6. Schematic diagram of (a) preparing composites and (b) representation of SWNTs-Graphene

In this regard, single-walled carbon nanotubes (SWNTs, hereafter) (P3-SWNT, average SWNT diameter of ~ 1.4 nm, length of 0.5-1μm, bundle diameter of 4-5 nm, Carbon Solutions, Inc.) are considered to improve the through-plane heat transport in composites, as a result of using the hybrid filler of one-dimensional structure. SWNTs were stirred with water-dispersible graphene at 70°C for 24 hours for combining hybrid fillers as shown in the figure 4.6. [52].

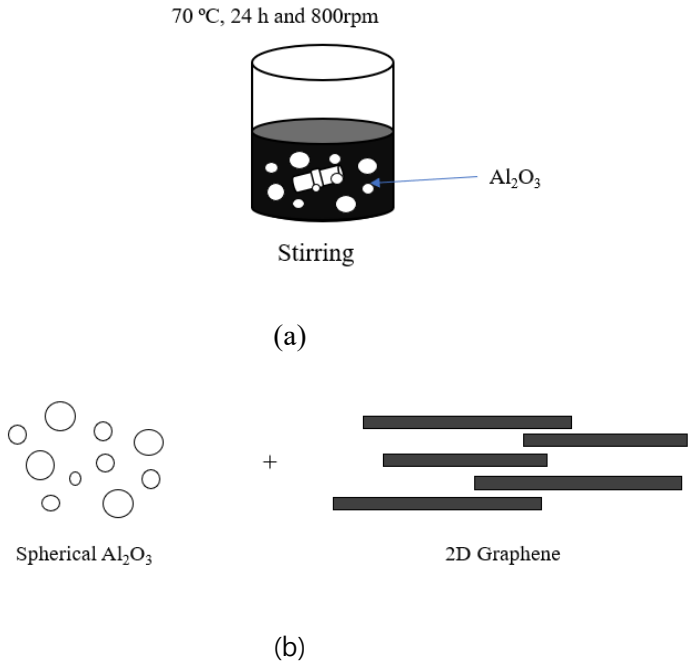

Figure 4.7. Schematic diagram of (a) preparing composites and (b) representation of Al_2O_3-Graphene

Also, this is the directed towards a more complete filling of the voids which must be occupied [30]. In this regards, conventional low aspect ratio micro-particle fillers were studied as shown in the figure 4.7. The hybrid filler was combined with a spherical particle of aluminum oxide (1-10μm, Sigma-Aldrich) and two-dimensional graphene [34]. The density of the used aluminum oxide is 4 g/cm^3. Also, aluminum oxide may have some other advantages because it can provide an electrical insulation [35].

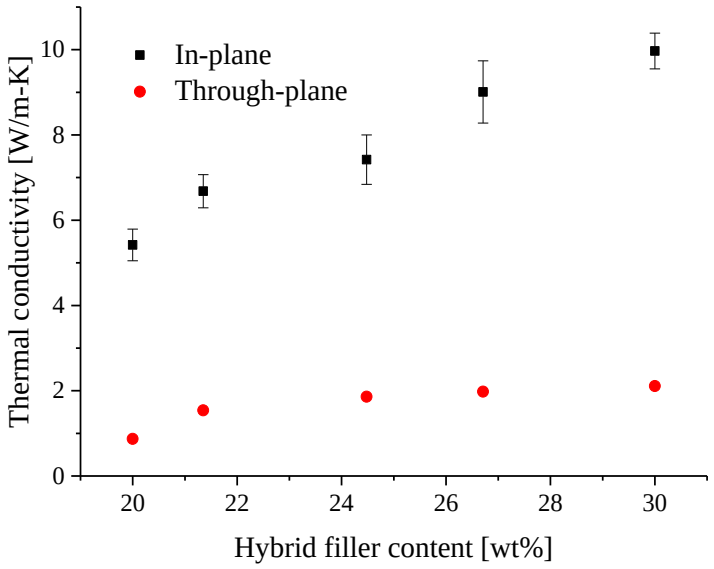

(a)

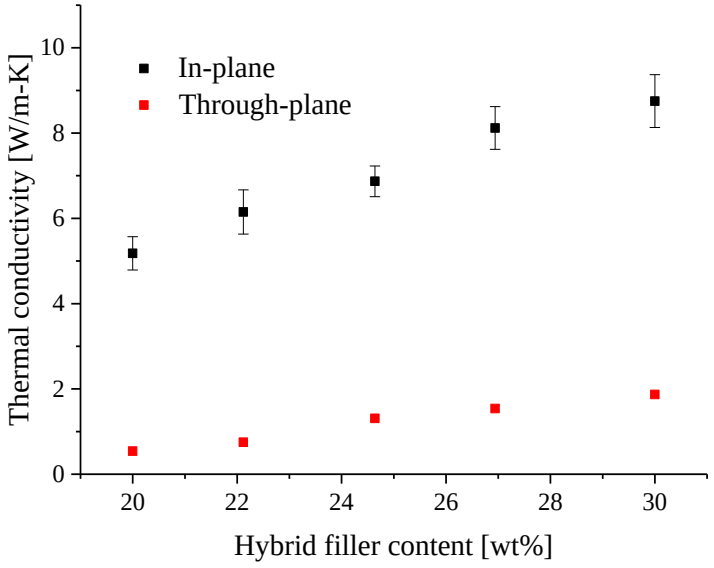

(b)

Figure 4.8. Effect of hybrid filler content on the thermal conductivities of (a) SWNTs-graphene and (b) Al_2O_3-graphene

The effects of hybrid filler of one-dimensional SWNTs or conventional low aspect ratio micro-particles of aluminum with two-dimensional graphene on the thermal performance of TIMs were investigated shown in the figure 4.8. Also, the through-plane thermal conductivities enhancement was investigated according to the hybrid filler contents. Figure shows the thermal conductivities of hybrid filler TIMs as a function of the mass fraction [47]. The thermal conductivity increased monotonically as the mass faction of the hybrid fillers. However, in the case of the hybrid filler of SWNTs and graphene, the increasing rate of the through-plane thermal conductivities over a mass fraction of 25 % decreases. This is due to the fact that at the higher loading of hybrid fillers, it caused the decreasing efficiency with a crossover of SWNTs. Also, it is expected to have percolation behavior in the through-plane heat transfer path [46].

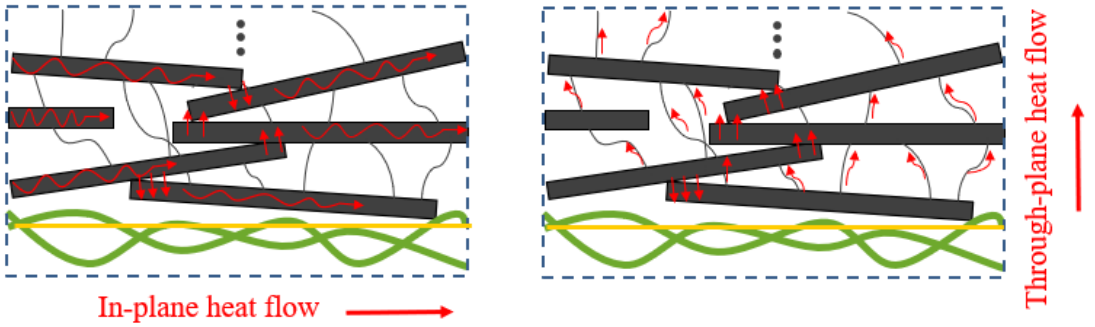

(a)

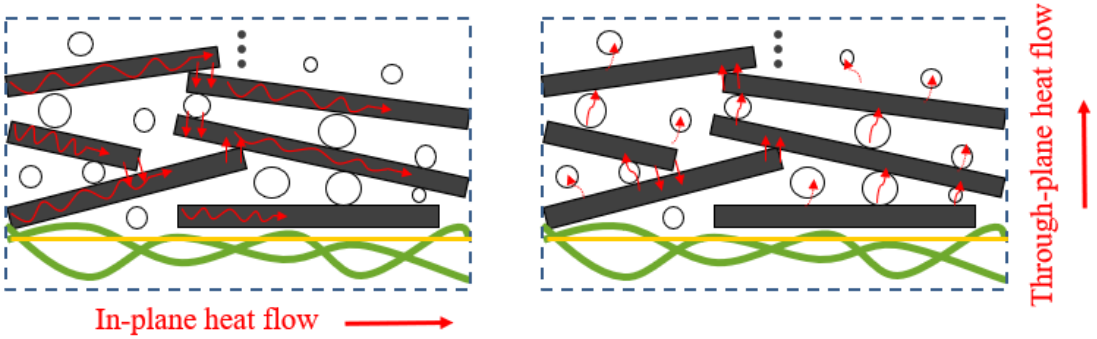

(b)

Figure 4.9. Comparison of heat transfer path for hybrid filler (a) SWNTs-graphene and (b) Al_2O_3-graphene

Figure 4.9. shows the heat transfer path for two types of hybrid fillers. In the case of hybrid fillers provide additional channels for the heat transport bypassing the cellulose matrix. Also, it can be confirmed that the end fragments of the bridging SWNTs are aligned along the graphene surfaces by the van der Waals attraction between the graphene structures. However, it would change the orientation of graphene cause the decreasing of in-plane thermal conductivities. Therefore, it is considered that studies for percolation threshold combining the hybrid fillers are important.

4.4. Electrical and mechanical properties

Table 4.4. Effect of coating process on the sheet resistance

Coating process	Paper	Thickness [mm]	Sheet resistance [ohm/sq]
Dip coating	Munken	0.18	631 ± 62
Dip coating	Matt	0.17	655 ± 57
Bar coating	Munken	0.13	565 ± 43
Bar coating	Matt	0.13	571 ± 50
Slot die coating	Munken	0.13	568 ± 38
Slot die coating	Matt	0.13	561 ± 30

Table 4.4. shows the electrical properties of graphene paper TIMs are investigated using the four-points probes measurement for measuring sheet resistance [28-29]. The measuring results of the sheet resistance about various coating process and paper type are shown table 4.3. It can be confirmed that relatively high sheet resistance of 655 ohm/sq for the dip coating process for Matt. On the other hand, in the case of the bar coating process, the sheet resistance is 515 ohm/sq for the Matt. For the slot die coating process, sheet resistance is the value of 508 ohm/sq and 511 ohm/sq for the Munken and Matt, respectively. For the effective electronic cooling for reducing the contact thermal resistance by using TIMs, relatively low electrical conductivity is required for the safety of the electronic device and thermal management application. Therefore, it can be confirmed that graphene paper TIMs show sufficient sheet resistance to be used as TIM.

Table 4.5. Effect of paper types on the sheet resistance

Paper	Thickness [mm]	In-plane thermal conductivity [W/m-K]
Bulgyeong	0.1	557 ± 28
Daerye	0.16	562 ± 31
Merit	0.13	578 ± 20
Aqua satin	0.15	607 ± 37
Wool paper	0.21	569 ± 36
New craft board	0.23	581 ± 45

Table 4.5. shows the results of sheet resistance according to six types of commercially-available papers. All of TIM was fabricated by using the slot die coating process and the coating thickness is 3 mm-thick regardless of paper types. As a measurement result of the sheet resistance, it is over 500 ohm/sq in all cases. It is also confirmed that it has the sufficient value of sheet resistance to be used as TIMs as with the previous results.

Mechanical properties can be another important factor in applying the thermal management system for using graphene paper TIMs.

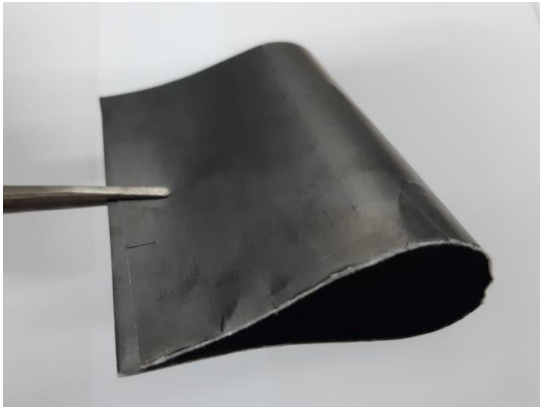

Figure 4.10. Flexibility of graphene-paper-based TIM

Firstly, the graphene paper TIMs has flexibility and it has the advantage that it can be applied by deforming into a desired shape according to the thermal management application as shown in the figure 4.10. [36]. The flexural strength of the paper is 138 MPa which is more than 40 % higher than the flexural strength 96 MPa of the commercially-available graphite sheet.

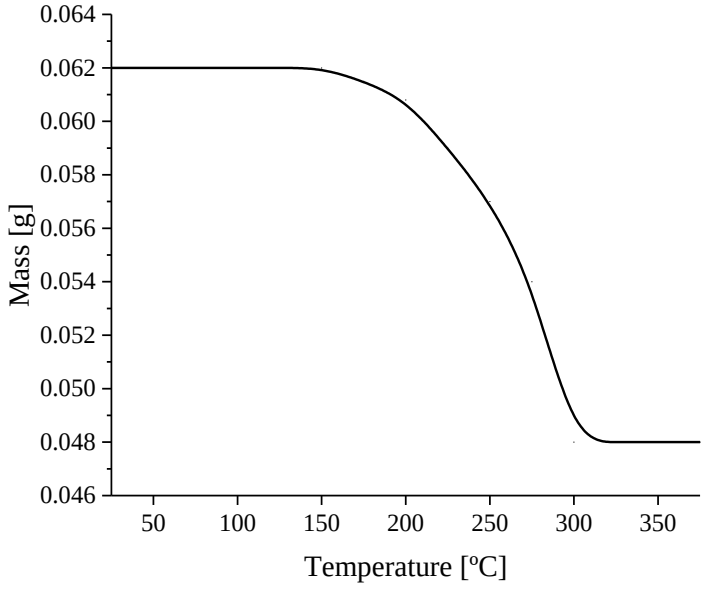

Figure 4.11. Thermal stability

Also, for the evaluation of thermal stability, the figure 4.11 shows the mass reduction of graphene paper TIMs is measured according to the temperature variation from 25 to 350℃ [37]. As a results, it is confirmed that the thermal stability is maintained in the range of over 120℃ at which the TIMs is normally used for the thermal degradation.

(a)

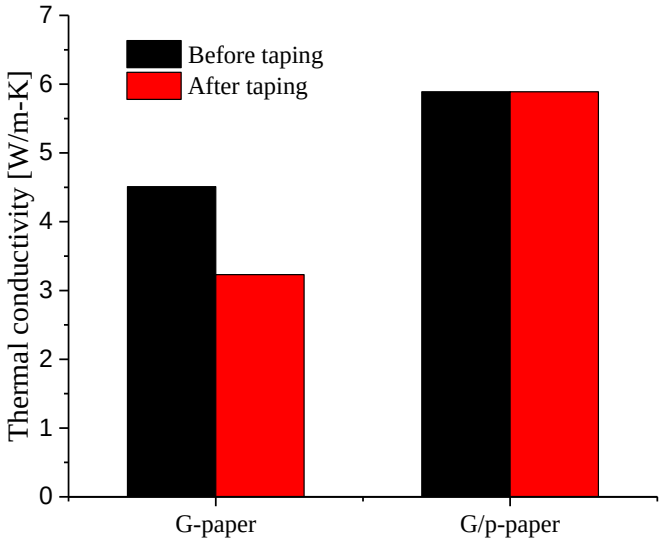

(b)

Figure 4.12. Coating stability for G-paper and G/p-paper of (a) after the scotch-tape tests and (b) thermal conductivities variation before and after the tests.

Also, the surface durability and adhesion are investigated through experiments in which the scotch-tape is detached repeatedly about 10 times shown in the figure 4.12. [21]. In case of G-Paper, coating surface is detached with scotch-tape test over 7 times. However, in the G/P-Paper is not greatly affected by the peeled off teat using scotch tape. It is because that improved surface durability and superior adhesion properties using co-polymer are the effect on the interaction of strong hydrogen bonding with copolymer and the hydroxyl group, -OH-, and the carboxyl group, -COOH- and -CH3COO- with cellulose and graphene. Also, the variation of thermal conductivity by testing scotch-

tape is detached over 10 times for the two types of graphene paper TIMs. After detaching the scotch tape 10 times, the thermal conductivities of G-Paper sharply decreased from the 4.52 W/m-K to 3.26 W/m-K. However, in the case of the G/P-Paper, there is no variation in thermal conductivity and it is confirmed that it shows excellent surface durability. These results show that adhesion of conductive graphene layer from the paper brings enhancement between graphene, cellulose, and the copolymer. Also, the thermal conductivities are superior when using this copolymer. It was obvious that the G/P-Paper treated by copolymer showed two times higher thermal conductivity compared with the G-Paper. Consequently, these results show that it is possible to improve the adhesion between cellulose, copolymer, and graphene by using the P(VB-co-VA-co-VAc) copolymer for preventing detachment of conductive graphene flake from the cellulose matrix.

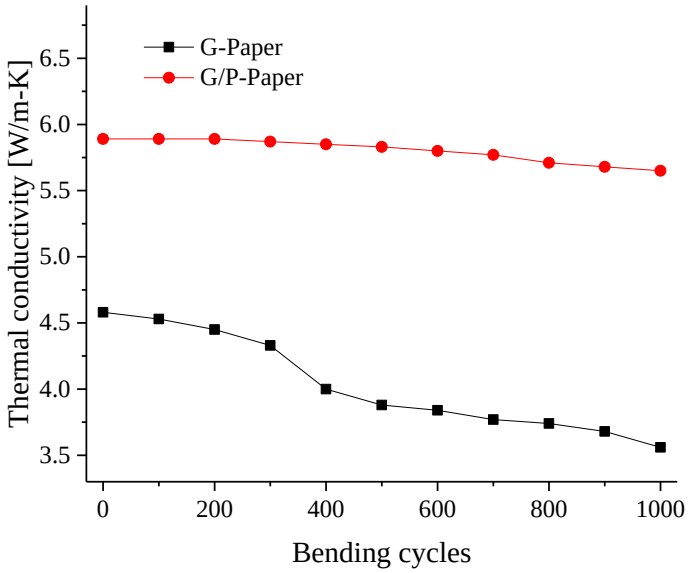

(a)

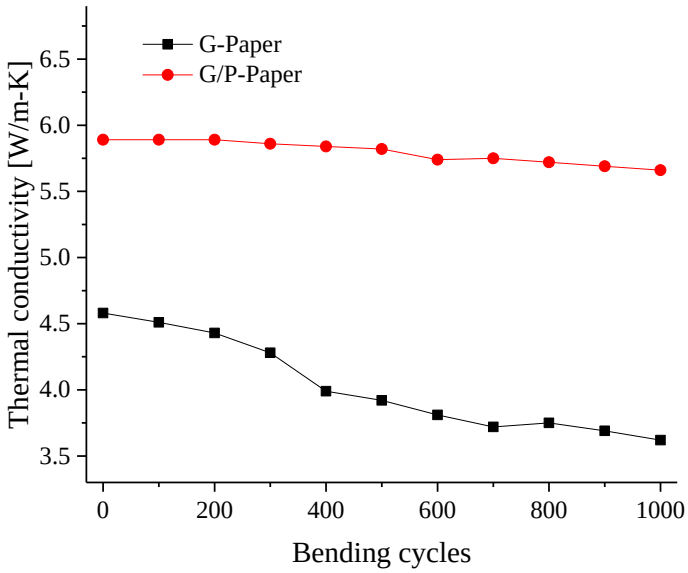

(b)

Figure 4.13. Mechanical stability of (a) compression and (b) tensile bending cycles.

Figure 4.13. show the results to further investigate the effects of mechanical strength of the graphene paper TIMs, 10,00 cycles in both compression and tensile stress are studied. The thermal conductivities of G-Paper decreased according to the compression and tensile bending cycles more sharply. And, the thermal conductivities of G/P-Paper shows almost constant value regardless of increasing bending cycles both the compression and tensile. This also confirmed that the thermal conductivities of G-Paper deteriorates more in the stress of the compression than in the tensile stress. Also, it can be confirmed that the G/P-Paper has superior durability for the stress of compression and tensile compared with the G-Paper. As described above, copolymer brings the enhancement of the adhesion with cellulose paper for the hydrogen bonding interaction and forms adhesive layer between the graphene and cellulose paper for preventing slipping between them. Therefore, the G/P-Paper has better durability when affected by compression and tension force. This means that graphene paper TIMs with flexibility is possible to be adopted for any application with required mechanical strength.

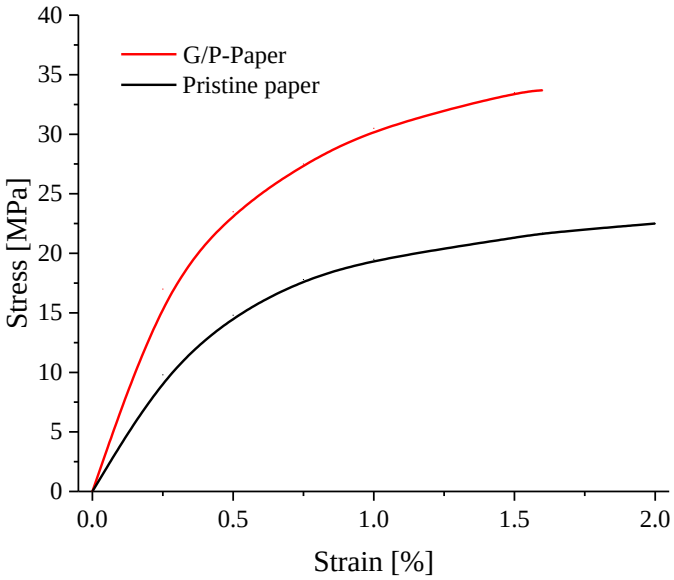

Figure 4.14. Stress-strain curves

Figure 4.14. show the capacity of graphene paper TIMs to the strain-stress curves of G/P-paper and pristine paper were investigated. The tensile strength of the papers decreased G/P-Paper of 33.8 MPa and the pristine paper of 21.2 MPa. As mentioned above, the copolymer strongly bonding interaction between the cellulose matrix, copolymer, and graphene with interactions of hydrogen bonding which prevents delamination in the G/P-Paper. The breaking strain of the papers decreased in the following value of pristine paper of 1.96 % and G/P-Paper of 1.68 %. It is confirmed that strain is less than 2 % even at a stress of 33.8 MPa. The breaking strain of the G/P-Paper was higher than that of the pristine paper. This implies that graphene paper with high flexibility can restore the overall flexibility of the cellulose paper.

Table 4.6. Surface roughness of graphene paper TIM

Types of paper	Surface roughness [*u*m]
Matt	1.89
Bulgyeong	2.06
Merit	1.32
New craft board	2.43

Table 4.6. shows the surface roughness of the graphene paper TIM according to the paper types. In general, the surface roughness range for low contact resistance is 1.27 to 1.5 *u*m. As a measurement results of four types of graphene paper TIM, it can be seen that Merit has a very low surface contact resistance to have surface roughness of 1.32 *u*m. It is assumed that Matt has a surface roughness that is acceptable value for 1.89 *u*m. Bulgyeong and New craft board are relatively large surface roughness. However, it is expected that the application for using the TIM will cause the improved surface area by pressing due to the porous structure and mechanical strength of the paper.

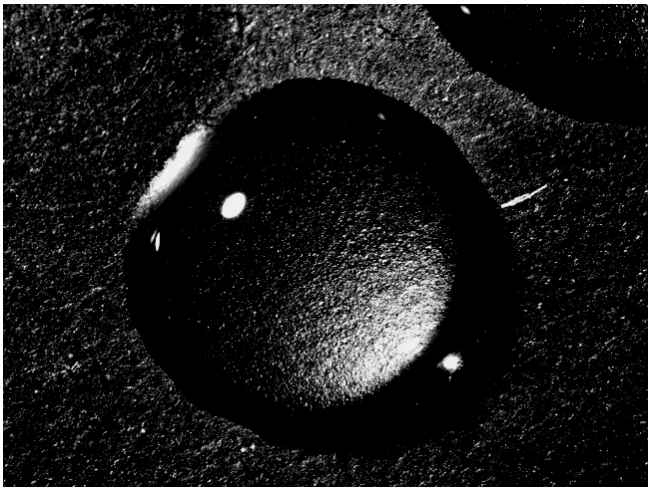

(b)

Figure 4.15. Surface wettability of graphene paper TIM

In general, applications such as semiconductor and electronics assembly where TIM is used are designed to maintain 40 to 60 % humidity to prevent degradation due to corrosion and delamination. It is expected that the change in the properties of the TIM in the corresponding humidity range will not cause and the thermal conductivity will be approximately maintained.

Also, graphene has hydrophobic characteristics as sown in the figure 4.15. The graphene paper TIM, which was expected to be weak to humidity due to the use of paper matrix, has graphene embedded in the porous structure of the paper and has a surface coated that it is acceptable result of durability for the humidity

Lastly, the hardness of commercially-available graphite sheet and graphene paper TIM have been compared. The result shows that pristine paper has higher hardness about 10 % than graphite sheet. Also, graphene paper TIM is expected to have a slightly higher value due to embedded graphene into the porous structure of paper. However, it is attributable that it shows the value within an allowable range in which the pressure condition to be used in TIM application. Compression rate of pristine paper and graphene paper TIM according to the pressure was measured by using digital multimeter. It can be confirmed that compression rate of pristine paper and graphene paper TIM are 30 ~ 40 % which is comparable to that of graphite sheet. In addition, the hardness of graphene paper TIM fabricated using Bulgyeong which is expected to be the softest in this study is considered to be much lower. Also, it is possible that using a paper matrix which is softer and low density than Bulgyeong, graphene paper TIM can be made and applied with sufficiently low hardness.

4.5. Comparison in the previous literature

Table 4.7. Comparison of properties in previous literatures

Author	Fabrication process	Thickness [mm]	In-plane thermal conductivity [W/m-K]	Through-plane thermal conductivity [W/m-K]
Our study	Slot die coating	0.19	7.32 ± 0.43	0.14 ± 0.02
Ding *et al.*	Hot pressing	0.2	9	Unknown
Yu *et al.*	LBL assembly	0.2	3.35	Unknown
Jiao *et al.*	VASA	0.1	6.618	0.053
Song *et al.*	VASA	0.05	5.73	Unknown

Finally, the graphene paper TIMs using the ink coating process is compared with other previous studies fabricated based on cellulose matrix and graphene filler as shown in the table 4.6. The comparison is investigated based on the fabricating process, the thickness of TIMs, the in-plane thermal conductivity, and the through-plane thermal conductivity. Firstly, our graphene paper TIMs show somewhat lower thermal conductivity than graphite sheet which is commercially-available sheet-typed TIMs. However, the graphite sheet requires very expensive equipment and a considerably high temperature for the fabrication process. Also, oxidation-reduction treatment of graphite is necessary and it is difficult to fabricate the scalable TIMs. However, our graphene paper TIMs is coated on the paper just using ink coating equipment. And, it is not sheet-typed TIMs but fabricated using paper, so it can be deformed freely and used for the application required very high flexibility and excellent mechanical properties. When Compared with the previous studies fabricated by using complex and time-consuming chemical process such as hot-pressing, vacuum-filtration, and LbL assembly, whereas our graphene paper TIMs can be fabricated using very easy, simple, and scalable ink coating process. Furthermore, thermal conductivity increased more than 100 times compared with the pristine paper with a thermal conductivity of 0.05 W/m-K. And, it also shows thin, flexible and comparable TIMs which have in-plane and through-plane thermal conductivities of 7.32 W/m-K and 0.14 W/m-K, respectively. In this regard, our graphene paper TIMs using ink coating process proposed a promising candidate for next-generation thermal interface materials with good thermal and mechanical properties.

5. Conclusion

Recently, according to the development of industry and technology, miniaturization of electronics results in very high heat generation per unit area. Also, thin and lightweight heat spreader has gained a significant attention in semiconductor industry. These important semiconductor parts must be mounted in a limited space based on the packaging technology, performance and lifetime must be secured at the same time. Therefore, how to effectively remove the heat generated from the parts is an important factor that can satisfy the thermal requirements. In these cooling modules, one of the major bottlenecks in the heat transfer path is the contact thermal resistance that occurs two mating rigid surfaces. Accordingly, it is indispensable to find the optimal solution for thermal management in the electronic package, TIMs are also regarded as an essential component in thermal management for reducing the thermal contact resistance. In regard to the TIMs, the flexibility, versatility, as well as thermal performance are considered as important properties.

In this study, a graphene paper based, thin and flexible TIMs have been successfully fabricated by incorporating commercially-available papers with water-dispersible graphene paste (WDG). Various types of commercially-available papers which have the different characteristics are used to fabricate the graphene paper TIMs via a simple and cost-effective ink coating process. Cellulose-based TIMs have been widely studied because of its lightweight, flexibility, and good mechanical properties. Also, graphene has been widely studied as a conductive filler because of its high thermal conductivity and mechanical properties. The mechanical strength is dramatically improved and the characteristics of graphene are adjusted by fabricating the highly thermally conductive material with cellulose. And, graphene is well absorbed in cellulose substrate and has a very high thermal conductivity characteristic in the horizontal direction. Also, graphene can be evenly dispersed in cellulose due to the formation of hydrogen bonds between them. Also, poly (vinyl butyral-co-vinyl alcohol-co-vinyl acetate) (P(VB-co-VA-co-VAc)) copolymer which is often used as an adhesive layer in the coating process is used for increasing the mechanical strength which is attributed to the strong hydrogen bonding interaction between the cellulose, copolymer, and graphene. The fabricated graphene paper TIMs show fairly-high mechanical properties which can significantly improve the thermal and mechanical properties, but it still remains in relatively high thermal conductivity.

The in-plane and through-plane thermal conductivities of the fabricated graphene paper TIMs are measured using the laser flash analysis, LFA technique. The measured in-plane thermal conductivities are of the order of 5 W/m-K, which corresponds to 100 times increase of thermal conductivity compared with the pristine paper, and the 0.19 mm thickness TIMs show the in-plane and through-plane thermal conductivities of 7.92 W/m-K and 0.14 W/m-K, respectively which shows a high value of thermal conductivity. On the other hand, the through-plane thermal conductivities are of the

order of 0.1 W/m-K which is relatively low value. The results show that in-plane thermal conductivities are relatively higher than through-plane thermal conductivities. Generally, thermal conduction are transferred by the vibrational energy of atoms and graphene can transfer more quickly for in-plane direction because of a strong bond with 2-dimensional. On the other hand, the van der Waals force between layered graphene are weak and through-plane thermal conductivities are relatively low. Also, the effect of the porosity of paper means a measure of the void spaces in a material to calculate the volume of void-space divided by total volume of material are investigated. As a result, the porosity which is characteristics of paper and thermal conductivities are somewhat proportional. It can be assumed that the paper with high porosity can absorb water-dispersible graphene well and it achieves the enhanced heat transfer path with cellulose. Also, the hybrid filler the utilization of multicomponent filler which include particles of different shapes and dimensions for improving the through-plane thermal conductivity is studied. The hybrid filler formulations result in a slight enhancement of the through-plane thermal conductivity by addition of micro particles fillers spherical or 1 dimensional configuration.

Also, the electrical properties of the graphene paper TIM are also tested by measuring the sheet resistance using the 4-point-probe measurement method. The measured sheet resistance are of the order of over 500 ohm/sq, which is sufficient values for TIM. In respect to the various mechanical properties, graphene paper TIM has the advantage that it can be transformed according to the system as its flexibility. And, the result of the mass reduction shows that the thermal stability is maintained in the range of over the TIM is normally used. Also, the tensile strength of graphene paper TIM is 33.82 MPa with strain is less than 2%.

From this study, the conclusions are as follows: i) The in-plane thermal conductivity of the graphene paper TIM is shown to be significantly higher than that of pristine paper of the order of 100 times. However, the through-plane thermal conductivity is not significantly enhanced by the graphene coating. ii) The slot die coating shows the best performance in terms of thermal conductivity, thinness, and evenness of thickness, over the dip coating and bar coating process, iii) The thermal conductivity of the graphene paper TIM is measured using laser flash technique according to paper types, mass faction of graphene, and thickness of TIMs, iv) The thermal conductivity of the graphene paper TIM is significantly affected by the paper types due to the difference of porosity, V) The sheet resistance and mechanical strength are measured and the graphene paper TIM shows good electrical and mechanical properties. Therefore, this study has developed an efficient approach to fabricate graphene paper thermal interface materials with good thermal and mechanical properties for a new possibility in thermal management systems.

REFERENCES

[1] S. Sun, S. Chen, X. Luo, Y. Fu, L. Ye, and J. Liu, “Mechanical and thermal characterization of a novel nanocomposite thermal interface materials for electronic packaging”, Microelectronics Reliability, Vol. 56, pp. 129-135, 2016.

[2] L. Maguire, M. Behnia, G. Morrison, “Systematic evaluation of thermal interface materials-a case study in high power amplified design”, Microelectronics Reliability, Vol. 45, pp. 711-725, 2005.

[3] A. Yu, P. Ramesh, M. E. Itkis, E. Bekyarova and R.C. Haddon, “Graphite nanoplatelet-epoxy composite thermal interface materials, The Journal of Physical Chemistry Letters C, Vol 111, pp. 7565-7569, 2007.

[4] J.P. Gwinn, R.L. Webb, “Performance and testing of thermal interface materials”, Microelectronics Journal, Vol. 34, pp. 215-222, 2003.

[5] B.A. Cola, X. Xu, T.S. Fisher, M.A. Capano, and P.B. Amama, “Carbon nanotube array thermal interfaces for high-temperature silicon carbide devices”, Nanoscale and Microscale Thermophysical Engineering, Vol. 12, pp. 228-237, 2008.

[6] S. Shen, A. Henry, J. Tong, R. Zheng and G. Chen, “Polyethylene nanofibers with very high thermal conductivities”, Nature Nanotechnology, Vol. 7, pp. 251-255, 2010.

[7] Y. Gao and J. Liu, “Gallium-based thermal interface material with high compliance and wettability”, Applied Physics A, Vol. 107, pp. 701-708, 2012.

[8] A. Rai and A.L. Moore, “Enhanced thermal conduction and influence of interfacial resistance within flexible high aspect ratio copper nanowire/polymer composites”, Composites Science and Technology, Vol. 144, pp. 70-78, 2017.

[9] N. Song, X. Hou, L. Chen, S. Cui, L. Shi and P. Ding, “A green plastic constructed from cellulose and functionalized graphene with high thermal conductivity”, ACS Applied Materials and Interfaces, Vol. 9 pp. 17914-17922, 2017.

[10] G. Li, X. Tian, X. Xu, C. Zhou, J. Wu, Q. Li, L. Zhang, F. Yang and Y. Li, “Fabrication of robust and highly thermally conductive nanofibrillated cellulose/graphite nanoplatelets composite papers”, Composites Science and Technology, Vol. 138 pp. 179-185, 2017.

[11] G. Li, X. Tian, X. Xu, C. Zhou, J. Wu, Q. Li, and L. Zhang, “Fabrication of robust and highly thermally conductive nanofibrillated cellulose/graphite nanoplatelets composite papers”, Composites Science and Technology, Vol. 138, pp. 179-185, 2017.

[12] N. Song, D. Jiao, S. Cui, X. Hou, P. Ding and L. Shi, “Highly anisotropic thermal conductivity of layer-by-layer assembled nanofibrillated cellulose/graphene nanosheets hybrid films for thermal management”, ACS Applied Materials and Interfaces, Vol. 9 pp. 2924-2932, 2017.

[13] S. Wang, Y. Cheng, R. Wang, J. Sun, and L. Gao, “Highly Thermal Conductive Copper Nanowire Composites with Ultralow Loading: Toward Applications as Thermal Interface Materials”, ACS Applied Materials and Interfaces, Vol. 6, pp. 6481-6486, 2014.

[14] N. Song, S. Cui, D. Jiao, X. Hou, P. Ding and L. Shi, “Layered nanofibrillated cellulose hybrid films as flexible lateral heat spreaders: The effect of graphene defect”, Carbon, Vol. 115, pp. 338-346, 2015.

[15] N. Song, D. Jiao, P. Ding, S. Cui, S. Tang and L. Shi, “Anisotropic thermally conductive flexible films based on nanofibrillated cellulose and aligned graphene nanosheets”, Journal of Materials Chemistry C, Vol. 4, pp. 305-314, 2016.

[16] F. Wang, L.T. Drzal, Y. Qin, and Z. Huang, “Multifunctional graphene nanoplatelets/cellulose nanocrystals composite paper”, ACS Composites Part B, Vol. 79, pp. 521-529, 2015.

[17] Y. Yao, X. Zeng, G. Pan, J. Sun, J. Hu, Y. Huang, R. Sun, J.B. Xu, and C.P. Wong, "Interfacial engineering of silicon carbide nanowire/cellulose microcrystal paper toward high thermal conductivity", ACS Applied Materials and Interfaces, Vol. 8, pp. 31248-31255, 2016.

[18] J. Hansson, M.J. Nilsson, L. Ye, and J. Liu, "Novel nanostructured thermal interface materials: a review", International Materials Reviews, Vol. 63, Issue 1, pp. 22-45, 2018.

[19] H. Zhu, Y. Li, Z. Fang, J. Xu, F. Cao, J. Wan, C. Preston, B. Yang and L. Hu, "Highly thermally conductive papers with percolative layered boron nitride nanosheets", ACS Nano, Vol. 8, Issue 4, pp. 3606-3613, 2014.

[20] P. Anithambigai, D. Mutharasu, L.H. Huong, T. Zahner, and D. Lacey, "Synthesis and thermal analysis of aluminum nitride filled epoxy composites and its effective application as thermal interface material for LED applications", Mater Electron, Vol. 25, pp. 4814-4821, 2014.

[21] K.W. Kim, J.H. Kim, S. Cho, K. Shin, and S.H. Kim, "Scalable high-performance graphene paper with enhanced electrical and mechanical properties", Thin Solid Films, Vol. 632, pp. 50-54, 2017.

[22] V. Goyal, and A.A. Balandin, "Thermal properties of the hybrid graphene-metal nano-micro-composites: Applications in thermal interface materials, Applied Physics Letter, Vol. 100, 2012.

[23] Y.K. Kim, J.Y. Chung, J.G. Lee, Y.K. Baek, and P.W. Shin, "Synergistic effect of spherical Al2O3 particles and BN nanoplates on the thermal transport properties of polymer composites", Composites Part A, Vol. 98, pp. 184-191, 2017.

[24] X. Tian, M.E. Itkis, and R.C. Haddon, "Application of Hybrid Fillers for Improving the Through-Plane Heat Transport in Graphite Nanoplatelet-Based Thermal Interface Layers", Scientific Reports, 5:13108, 2015.

[25] Y. Xu, and D.D.L. Chung, “Increasing the thermal conductivity of boron nitride and aluminum nitride particle epoxy-matrix composites by particle surface treatments”, Composite Interfaces, Vol. 7. Issue 4, pp. 243-256, 2000.

[26] P. Lv, X.W. Tan, K.H. Yu, R.L. Zheng, J.J. Zheng, and W. Wei, “Super-elastic graphene/carbon nanotube aerogel: A novel thermal interface material with highly thermal transport properties”, Carbon, Vol. 99, pp. 222-228, 2016.

[27] R. Viswanath, V. Wakharkar, A. Watwe, and V. Lebonheur, “Thermal performance Challenges from Silicon to Systems”, Intel Technology Journal, 2000.

[28] K.S. Novoselov, A.K. Geim, S.V. Morozov, D. Jiang, Y. Zhang, S.V. Dubonos, I.V. Grigorieva, and A.A. Firsov, “Electric Field Effect in Atomically Thin Carbon Films”, Science, Vol. 306, Issue 22, 2004.

[29] C.A. Martin, J.K. Sandler, A.H. Windle, M.K. Schwarz, W. Bauhofer, K. Schulte, and M.S. Shaffer, “Electric field-induced aligned multi-wall carbon nanotube networks in epoxy composites”, Polymer, Vol. 46, pp. 877-886, 2005.

[30] J. Xu, T.S. Fisher, “Enhanced of thermal interface materials with carbon nanotube arrays”, International Journal of Heat and Mass Transfer, Vol. 49, pp. 1658-1666, 2006.

[31] A. Yu, P. Ramesh, M.E. Itkis, E. Bekyarova, and R.C. Haddon, “Graphite Nanoplatelet-Epoxy Composite Thermal Interface Materials”, The Journal of Physical Chemistry C Letters, Vol. 111, pp. 7565-7569, 2007.

[32] K. Zhang, Y. Chai, M.M. Yuen, D.G. Xiao, and P.C. Chang, “Carbon nanotube thermal interface material for high-brightness light-emitting-diode cooling”, Nanotechnology, Vol. 19, 2008.

[33] S. Narumanchi, M. Mihalic, and K. Kelly, “Thermal Interface Materials for Power Electronics Applications”, IEEE, 2008.

[34] W. Lin, K.S. Moon, S. Zhang, Y. Ding, J. Shang, M. Chen, and C.P. Wong, “Microwave Makes Carbon Nanotubes Less Defective”, ACS Nano, Vol. 4, Issue 3, 2010.

[35] Z. Yuan, J. Yu, Z. He, X. Wu, B. Rao, S. Lu, and Nan Jiang, “Improved Thermal Properties of Epoxy Composites Filled with Thermotropic Liquid Crystalline Epoxy Grafted Aluminum Nitride”, Fibers and Polymers, Vol. 15, Issue 12, pp. 2581-2590, 2014.

[36] Y. Chai, J. Gong, K. Zhang, P.C. Chang, and M.F. Yuen, “Flexible transfer of aligned carbon nanotube films for integrating at lower temperature”, Nanotechnology, Vol 18, pp, 2007.

[37] M. Sharma, and D.L. Chung, “Solder-graphite Network Composite Sheets as High-Performance Thermal Interface Materials”. Journal of Electronic Materials, Vol. 44, Issue 3, 2015.

[38] N.H. Inai, A.E. Lewandowska, O.R. Ghita, and S.J. Eichhorn, “Interfaces in polyethylene oxide modified cellulose nanocrystal – polyethylene matrix composites”, Composites Science and Technology, Vol. 154, pp. 128-135, 2018.

[39] D. Zhu, Y. Qi, W. Yu, L. Chen, M. Wang, and H. Xie, “Enhanced Thermal Conductivity for Graphene Nanoplatelets/Epoxy Resin Composites”, Journal of Thermal Science and Engineering Applications, Vol. 10, 2018.

[40] R. Gulfam, W. Zhu, L. Xu, I.I. Cheema, P. Sheng, G. Zhao, and Y. Deng, “Design, fabrication and numerical analysis of compact thermal management system integrated with composite phase change material and thermal bridge”, Energy Conversion and Management, Vol. 156, pp. 25-33, 2018.

[41] K. Pashayi, H.R. Fard, F. Lai, S. Iruvanti, J. Plawsky, and T.B. Tasciuc, “High thermal conductivity epoxy-silver composites based on self-constructed nanostructured metallic networks”, Journal of Applied Physics, Vol. 111, 2012.

[42] S.N. Leung, M.O. Khan, E. Chan, H. Naguib, F. Dawson, V. Adinkrah. L.L. Hauward, “Analytic modeling and characterization of heat transfer in thermally conductive polymer composites filled with spherical particulates”, Composites Part B, Vol. 45, pp. 43-49, 2013.

[43] N.L. Rodriguez, W. Thielemans, and A. Dufresne, “Sisal cellulose whiskers reinforced polyvinyl acetate nanocomposites”, Cellulose, Vol. 13, pp. 261-270, 2006.

[44] C. Zhang, R. Cha, L. Yang, K. Mou, and X. Jiang, “Fabrication of cellulose/graphene paper as a stable-cycling anode materials without collector”, Carbohydrate Polymers, Vol. 184, pp. 30-36, 2018.

[45] J. Hong, J. Lee, C.K. Hong, and S.E. Shim, “Effect of dispersion state of carbon nanotube on the thermal conductivity of poly(dimethyl siloxane) composites”, Current Applied Physics, Vol. 10, pp. 359-363, 2010.

[46] M. Obori, S. Nita, A. Miura, and J. Shiomi, “Onsite synthesis of thermally percolated nanocomposite for thermal interface material”, Journal of Applied Physics, Vol. 119, Issue 5, 2016.

[47] T. Tong, Y. Zhao, L. Delzeit, A. Kashani, M. Meyyappan, and A. Majumdar, “Dense Vertically Aligned Multiwalled Carbon Nanotube Arrays as Thermal Interface Materials”, IEEE Transactions on Components and Packaging Technologies, Vol. 30, Issue 1, pp. 2008.

[48] P.G. Ren, X.H. Si, Z.F. Sun, F. Ren, L. Pei, and S.Y. Hou, “Synergistic effect of BN and MWCNT hybrid fillers on thermal conductivity and thermal stability of ultra-high-molecular-weight polyethylene composites with a segregated structure”, Journal of Polymer Research, Vol. 23, Issue 21, 2016.

[49] Q. Liang, X. Yao, W. Wang, Y. Liu, and C.P. Wong, "A Three-Dimensional Vertically Aligned Functionalized Multilayer Graphene Architecture: An Approach for Graphene-Based Thermal Interfacial Materials", ACS Nano, Vol. 5, Issue 3, pp. 2392-2401, 2011.

[50] H. Wang, A.S. Tazebay, G. Yang, H.T. Lin, W. Choi, and C. Yu, "Highly deformable thermal interface materials enabled by covalently-bonded carbon nanotubes", Carbon, Vol. 106, pp. 152-157, 2016.

[51] Q. Lim C. Liu, and S. Fan, "Thermal Boundary Resistances of Carbon Nanotubes in Contact with Metals and Polymers", Nano Letters, Vol. 9, Issue 11, pp. 3805-3809, 2009.

[52] H. Huang, C. Liu, Y. Wu, and S. Fan, "Aligned Carbon Nanotube Composite Films for Thermal Management", Advanced Materials, Vol. 17, pp. 1652-1656, 2005